Latin American Journal of Solids and Structures
www.lajss.org

High Order Impact Elastic Analysis of Circular Thick Cylindrical Sandwich Panels Subjected to Multi-mass Impacts

Abstract

This study dealt with the dynamic model of composite cylindrical sandwich panels with flexible cores and simply supported boundary conditions under low velocity impacts of multiple large or small masses using a new improved higher order sandwich panel theory (IHSAPT). In-plane stresses were considered for the core and face sheets. Formulation was based on the first order shear deformation theory for the composite face sheets and polynomial description of the displacement fields in the core that was based on the second Frostig's model. Fully dynamic effects of the soft core and face-sheets were considered in this investigation. Impacts were assumed to occur simultaneously and normally over the top face-sheet with arbitrarily different masses and initial velocities. The contact forces between the panel and impactors were treated as the internal forces of the system. In this paper, nonlinear contact stiffness was linearized with a newly presented improved analytical method. Numerical results of the mentioned structures were compared with finite element model using ABAQUS code.

Keywords

Cylindrical sandwich panel; Low velocity impact; Spring-mass model; Modified Hertz's model.

K. Malekzadeh Fard [a] *
A. Veisi Ghorghabad [a]
A. H. Azarnia [a]
Faramarz Ashenai Ghasemi [b]

[a] Department of Structural Analysis and Simulation, Space research institute, MalekAshtar University of Technology, Tehran-Karaj Highway, Post box: 13445-768, Tehran, IRAN
[b] Faculty of Mechanical Engineering, Shahid Rajaee Teacher Training University (SRTTU), Lavizan, Postal Code: 16788-15811,Tehran, Iran.
F.a.ghasemi@srttu.edu
*Author email: kmalekzadeh@mut.ac.ir

http://dx.doi.org/10.1590/1679-78251758

Received 06.12.2014
Accepted 22.06.2015
Available online 07.07.2015

1 INTRODUCTION

One of the greatest concerns about composites is their behavior under the impact of foreign bodies. Structural strength is greatly reduced due to impact damage. Such damage is not easily apparent, but its effect on structural strength can be determined. In the past four decades, research papers and books have been published on the issue of impact. Especially in recent years, analytical solutions of low velocity impact have been developed. An analytical solution has been expanded about the impact response of simply supported anisotropic composite cylinder with a modified Hertzian law by Matemilola and Stronge (1997).Results of this paper showed that strain slowly decreased in the direction which had a relatively large modulus. An overview of the mathematical

models for low velocity impact on structures was done by Abrate (2001), in which a procedure was presented to determine the type of impact and to select an appropriate model.
HooFatt and Park (2001) presented an analytical solution for the transient deformation of sandwich panels using mass model and Kirchhoff theory. Olsson (2001) proposed an engineering method for predicting the impact response and damage in sandwich panels. Impact response of laminated composite cylindrical shells was investigated by Krishnamurthy et al. (2001).Important results of the mentioned method were as follows:(a) Effect of impactor velocity was more than effect of the impactor mass on the contact force of the structure. (b) Impact-induced damage tended to increase with higher velocity of impact. (c) Effect of curvature was more significant when the curvature was high, and (d) Deflection and time of contact increased with decreasing the curvature.

Symbols and Abbreviations

Nomenclature	
E_m^i	effective elastic modulus of the ith impactor (m=j) and target structure (m=s)
$F_c^i(t), F^i(t)$	impact forces based on the linearized Hertzian and Hertzian contact laws, respectively,(i=1,2,...,N)
$F_c^i \max$	maximum impact force corresponding to ith impactor
h	sandwich structure thickness
h_t, h_c, h_b	thickness of the top face sheet, core and bottom face sheet, respectively
$I_n^i \ (i=t,b,c)$	the moments of inertia of the top and bottom face sheets and core
K_S	shear correction factor
K, U, W_{ext}	kinetic, strain and external works energy
K_c^i, K_c^{*i}	coefficients of the Hertzian and linearized Hertzian contact laws, respectively, (i=1,2,...,N)
K_{cl}^i	modified contact stiffness, (i=1,2,...,N)
K_g^i	impacted surface stiffness at the ith impact location
M_I^i	mass of the ith impactor
M_z^c	normal bending moments per unit length of the edge of the core
M_{eff}^s	effective mass of the target structure
$M_{xy}^i, M_{yx}^i, M_{xx}^i, M_{yy}^i$	bending and shear moments per unit length of the edge (i=t,b)
$M_{nxx}^c, M_{nxy}^c, M_{nyy}^c, M_{nyx}^c, M_{nxz}^c, M_{nyz}^c, M_{nxz}^{*c}, M_{nyz}^{*c}$	shear and bending moments per unit length of the edge of the core, (n=1,2,3)
n	exponent in the Hertzian contact law
N	number of layers and impactors

N^i	effective target structure mass to the ith impactor mass ratio
$\bar{N}^i_{xxj}, \bar{N}^i_{yyj}, \bar{N}^i_{xyj}$	the in-plane external loads in the longitudinal and transverse direction, respectively(i = t, b), (j=1,2)
$N^i_{xy}, N^i_{yx}, N^i_{xx}, N^i_{yy}$	in-plane and shear forces per unit length of the edge (i=t, b)
$N^c_{xz}, N^c_{yz}, N^{*c}_{xz}, N^{*c}_{yz}$	shear forces per unit length of the edge of the core
$q_j(x_i, y_i)$	impact forces over the (top or/and bottom) impacted face sheet (j=t, b)
Q^i_{xz}, Q^i_{yz}	shear forces in the face-sheets per unit edge length
R_{jt}, R_{jb}, R_{jc}	principal radii of curvature of middle surface of the top and bottom face sheets and the core (j=x, y)
R^i	radius of ith impactor
R^c_z	normal force per unit length of the edge of the core
$0-t$	time interval of analysis
$t^i{}_{\max}$	maximum contact time corresponding to ith impactor
u_k, v_k, w_k	unknowns of the in-plane displacements of the core (k=0,1,2,3)
u_c, v_c, w_c	displacement components of the core
u^i_0, v^i_0, w^i_0	displacement components of the face-sheets, (i = t, b)
$\ddot{u}_c, \ddot{v}_c, \ddot{w}_c$	acceleration components of the core
$\ddot{u}_{0j}, \ddot{v}_{0j}, \ddot{w}_{0j}$	acceleration components of the face-sheets, (j= t, b)
V^i_0	initial velocity of ith impactor
w^i_j	displacement of the ith impactor
(x_i, y_i)	ith impact location on the impactedface-sheet, (i=1,2,...,N)
$Z^i_2(t), Z^i_1(t)$	deflections of the impacted surface and ith impactor at ith impact point
Greek letters	
$\alpha^i(t)$	contact indentation for the ith impactor
δ	variational operator
δ^i_1	static displacement of the impacted surface at the ith impact location
ν_{12}, ν_{21}	Poisson's ratio
ν^i_m	effective Poisson's ratio of the ith impactor (m=j) and target structure(m=s)
ρ_t, ρ_b, ρ_c	material densities of the face-sheets and the core
σ^j_{ii}	normal stress in the face sheets, (i=x,y), j=(t,b)
σ^c_{ii}	normal stress in the core, (i=x,y,z)
$\tau^j_{xy}, \tau^j_{xz}, \tau^j_{yz}$	shear stress in the face sheets, j=(t,b)
$\tau^c_{xy}, \tau^c_{xz}, \tau^c_{yz}$	shear stresses in the core

$\varepsilon^i_{0xx}, \varepsilon^i_{0xy}, \varepsilon^i_{0yy}, \varepsilon^i_{0xz}, \varepsilon^i_{0xz}$	the mid-plane strain components, (i=t,b)
$\varepsilon^c_{zz}, \varepsilon^c_{xx}, \varepsilon^c_{yy}$	normal strains components of the core
$\gamma^c_{xz}, \gamma^c_{yz}, \gamma^c_{xy}$	shear strains components of the core
ω^i_1, ω^i_2	natural frequencies of spring-mass system corresponding to the ith impactor
ω_f	the lowest natural frequency of the structure
ϕ_1 , ϕ_2	rotation of the normal section of mid surface along x, y
ϕ_n	rotations about the transverse normal to the face sheets
$\kappa^i_{xx}, \kappa^i_{yy}$	the curvatures in the x and y-directions, respectively, (i=t, b)
κ^i_{xy}	the torsion curvature of the face-sheets, (i=t, b)

Analytical and finite element methods were considered for impact response of a laminated composite cylindrical shell by Krishnamurthy et al. (2003).In analytical method, the solution was obtained by means of an alternative numerical procedure incorporating the non-linear Hertz contact law. Such method also provided information as the natural frequencies of impacted shell which helped in obtaining appropriate mesh and time step sizes for finite element method.A new equivalent three-degree-of-freedom (TDOF) spring–mass–damper (SMD) model and a new analytical procedure about impact were presented by K. Malekzadeh et al. (2006), which predicted the effect of low velocity impact on sandwich panels with soft/stiff flexible core. Such an analytical solution describes the history of the contact force, displacement of the impactor, and displacement of the panel in the transverse direction in terms of material properties, structural mass, impactor mass and velocity, and structural damping. Contact force history by impact on composite sandwich plates can be obtained using general-purpose commercial FEM software using the spring element by Choi (2006).The advantage of this method is that no coding process is necessary for the development of additional FEM program. Dynamic response of the composite cylindrical shells under initial stresses and impulse effects were studied by Khalili et al. (2009). They studied the effect of internal pressure on the natural frequencies, and dynamic response of composite shells and compared them with those of the axial force.

Low velocity impact damage in thick composite cylinders using MT162 progressive damage model implemented in LS-Dyna were modeled by Kang et al. (2010). For this finite element method ,various impact energies were applied with different impact velocities ,and the results including deformation ,damage progression etc. as a function of impact energy were discussed.
A review of the previous and current progress of studies on the dynamic response of composite sandwich panels which is subjected to low velocity impact was made by G. B. Chai and S. Zhu (2011). Also, the effect of factors on the response, classification of response, and failure modes of the composite structures subjected to low velocity impact was discussed. Hossini et al. (2011) proposed an analytical approach for the contact problem of sandwich panels indented by a flat-ended cylinder. In this paper, using minimum total potential energy principle and contact law was improved. Also, shear extension coupling term was considered in this analysis. The dynamic

response of laminated composite cylindrical shell subjected to pure impact numerically was presented by Firouzabadi et al. (2012). In that paper, the impact of steel ball on cylinder was modeled by ABAQUS software as a point load .They studied the amount of radial deflection and contact force for whole period of contact motion.

Recently, a higher order model for the analysis of circular composite sandwich panel shells subjected to low velocity impact loads was presented by Khalili et al. (2013). In the mentioned paper, for the interaction between the impactor and structure, the spring-mass model was applied. Different higher order shell theories for low velocity impact analysis of circular cylindrical shells were evaluated by Davar et al. (2013).In order to investigate contact force history, a new two-degree-of-freedom spring-mass model was used. Further, metal volume fraction and fiber-metal laminate lay-up on the impact velocity were investigated. A comprehensive of past and current works published on the dynamic response of fiber-metal laminates subjected to low velocity impact was fulfilled by Chai (2014).This review included experimental, numerical, and analytical works on the low velocity impact of fiber-metal laminates.

Experimental and numerical investigation of lattice-walled cylindrical under impact loading were studied by Damghani et al. (2015).The drop hammer setup was used for experimental test and the numerical simulations were conducted by Abaqus.Type of results, including collapse, force-displacement diagrams, the crushing length and the absorbed energy were investigated. Few studies have been conducted about low velocity impact on cylindrical sandwich panels.

In this paper, impact analysis of the cylindrical composite/metal sandwich structures was expressed based on the first order shear deformation theory for the face-sheets and second Frostig's model for the core. For such a core, the vertical flexibility of the core must take into account, since this flexibility had an effect on stress and displacement fields of the face-sheets and produces nonlinear distribution of in-plane and vertical displacements of the core. In mathematical formulation, the Hamilton's principle was used to derive the governing equations of motion along with the appropriate boundary conditions. To predict the impact force and other parameters, the modified spring-mass system with two degrees of freedom (TDOF model) and nonlinear form of Hertz's contact force model (complete solution model) were used.

2 Formulations of Cylindrical Composite Sandwich Panels

Consider a cylindrical composite sandwich panel which is composed of two laminated face-sheets. Thickness of the top face-sheet, bottom face-sheet, and core is h_t, h_b , and h_c,respectively. The panel is assumed to have the radius of R and length of L, as shown in Fig. 1.1.Below, indices t and b refer to the top and bottom face-sheets of the panel, respectively. The assumptions used in the present analysis are followed by those encountered in linear elastic small deformation. u, v, and w are displacement components in the axial, tangential, and radial directions, respectively. Based on the first shear deformation theory, the displacements u, v, and w of the face-sheets with small linear displacements are expressed through the following relations (2004):

$$\begin{aligned} u_i(x,z,\theta,t) &= u_0^i(x,\theta,t) + z_i \psi_x^i(x,\theta,t) \\ v_i(x,z,\theta,t) &= v_0^i(x,\theta,t) + z_i \psi_\theta^i(x,\theta,t) \\ w_i(x,z,\theta,t) &= w_0^i(x,\theta,t) \quad ;(i=t,b) \end{aligned} \tag{1}$$

$\psi_x^i, \psi_y^i (i = t,\ b)$ are the rotation components of the transverse normal along the X and Y axes of the mid-plane of the top and bottom face-sheets; u_0^i, v_0^i, and w_0^i $(i=t,b)$ are displacements in X and Y directions and the vertical deflection of the top and bottom face-sheets, respectively; Z_i is vertical coordinate of each face-sheet, which is shown using $(i = t,\ b)$ and is measured upward from the mid-plane of each face-sheet (Figure 1.1). Kinematic equations for the strains of the face-sheets are as follows:

$$\begin{aligned} &\varepsilon_{xx}^i = \varepsilon_{0xx}^i + z_i \kappa_{xx}^i \quad , \qquad \varepsilon_{\theta\theta}^i = \varepsilon_{0\theta\theta}^i + z_i \kappa_{\theta\theta}^i , \quad \varepsilon_{zz}^i = 0 \\ &\gamma_{x\theta}^i = 2\varepsilon_{x\theta}^i = \varepsilon_{0x\theta}^i + z_i \kappa_{x\theta}^i , \quad i = t,b \\ &\gamma_{xz}^i = 2\varepsilon_{xz}^i = \varepsilon_{0xz}^i \quad , \qquad \gamma_{\theta z}^i = 2\varepsilon_{\theta z}^i = \varepsilon_{0\theta z}^i \end{aligned} \tag{2}$$

In which:

$$\begin{aligned} &\varepsilon_{0xx}^i = \frac{\partial u_0^i}{\partial x}, \qquad \varepsilon_{0yy}^i = \frac{\partial v_0^i}{R_i \partial \theta} + \frac{w_0^i}{R_i}, \qquad \varepsilon_{0xy}^i = \frac{\partial v_0^i}{\partial x} + \frac{\partial u_0^i}{R_i \partial \theta} \\ &\varepsilon_{0xz}^i = \frac{\partial w_0^i}{\partial x} + \psi_x^i, \qquad \varepsilon_{0yz}^i = \frac{\partial w_0^i}{R_i \partial \theta} + \psi_\theta^i - \frac{v_0^i}{R_i} \\ &\kappa_{xx}^i = \frac{\partial \psi_x^i}{\partial x}, \qquad \kappa_{yy}^i = \frac{\partial \psi_\theta^i}{R_i \partial \theta}, \qquad \kappa_{xy}^i = \frac{\partial \psi_\theta^i}{\partial x} + \frac{\partial \psi_x^i}{R_i \partial \theta} \end{aligned} \tag{3}$$

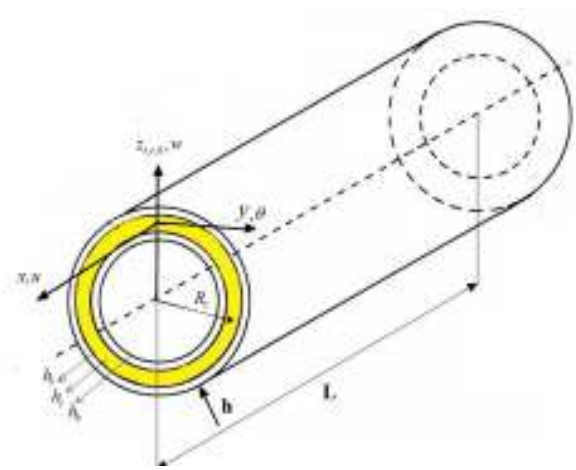

Figure 1.1: A cylindrical composite sandwich panel along with the panel coordinates and dimensions.

For the displacement fields of the core, the cubic pattern through the core thickness is considered. But, for vertical displacement of the core, the field has a quadratic form (2004).

$$\begin{cases} u_c(x,\theta,z,t) = u_0^c(x,\theta,t) + z_c u_1^c(x,\theta,t) + z_c^2 u_2^c(x,\theta,t) + z_c^3 u_3^c(x,\theta,t) \\ v_c(x,\theta,z,t) = (1+\dfrac{z}{R_c}) v_0^c(x,\theta,t) + z_c v_1^c(x,\theta,t) + z_c^2 v_2^c(x,\theta,t) + z_c^3 v_3^c(x,\theta,t) \\ w_c(x,\theta,z,t) = w_0^c(x,\theta,t) + z_c w_1^c(x,\theta,t) + z_c^2 w_2^c(x,\theta,t) \end{cases} \tag{4}$$

u_k^c, v_k^c (k=0, 1, 2, 3) are the unknowns of the in-plane displacements of the core, w_k^c (k=0, 1, 2) are the unknowns of vertical displacement, and R_c is the curvature radii of the top face-sheet. It is assumed that the accelerations and velocities of the core have the same distributions. Kinematic relations of the core for a cylindrical sandwich panel that are based on small deformations are:

$$\begin{aligned} &\varepsilon_{xx}^c = \frac{\partial u_c}{\partial x}, \quad \varepsilon_{\theta\theta}^c = \frac{1}{(1+z/R_c)}\left(\frac{\partial v_c}{R_c \partial\theta} + \frac{w_c}{R_c}\right) \\ &\gamma_{x\theta}^c = 2\,\varepsilon_{x\theta}^c = \frac{\partial v_c}{\partial x} + \frac{1}{(1+z/R_c)}\frac{\partial u_c}{R_c \partial\theta} \\ &\gamma_{xz}^c = 2\varepsilon_{xz}^c = \frac{\partial w_c}{\partial x} + \frac{\partial u_c}{\partial z} \\ &\gamma_{\theta z}^c = 2\varepsilon_{\theta z}^c = \frac{1}{(1+z/R_c)}\left(\frac{\partial w_c}{R_c \partial\theta} - \frac{v_c}{R_c}\right) + \frac{\partial v_c}{\partial z} \end{aligned} \tag{5}$$

By substituting displacement fields of the core, namely Eq. (4) in Eq. (5), strains of the core can be obtained. Compatibility conditions are based on perfect bonding between the core and face-sheets and the top and bottom face-sheet–core interfaces are:

$$\begin{cases} u_c(z=z_{ci}) = u_0^i + \dfrac{1}{2}(-1)^k h_i \psi_x^i \\ v_c(z=z_{ci}) = v_0^i + \dfrac{1}{2}(-1)^k h_i \psi_\theta^i \qquad ;i=t \rightarrow \left(k=1\,;\, z_{ct} = \dfrac{h_c}{2}\right) \\ w_c(z=z_{ci}) = w_0^i \qquad\qquad ;i=b \rightarrow \left(k=0\,;\, z_{cb} = -\dfrac{h_c}{2}\right) \end{cases} \tag{6}$$

Due to compatibility conditions, the number of unknowns of the core is reduced. As a result, unknowns are $u_0^c, u_1^c, v_0^c, v_1^c$ and w_0^c. Therefore, all unknowns for a circular cylindrical composite sandwich panel in a general form are fifteen as follows:

$$\left\{u_0^t, v_0^t, w_0^t, \psi_x^t, \psi_y^t, u_0^b, v_0^b, w_0^b, \psi_x^b, \psi_y^b, u_0^c, u_1^c, v_0^c, v_1^c, w_0^c\right\}$$

2.1 Governing Equation of Motions of the System

Derivation of the governing equations and boundary conditions is based on the Hamilton's principle of the minimization of the Lagrangian, as follows:

$$\int_0^T \delta L dt = \int_0^T [\delta K - \delta U + \delta W_{ext}] dt = 0 \tag{7}$$

where δK denotes variation of the kinetic energy, δU is variation of the strain energy, and δW_{ext} shows variation of the potential energy due to the applied loads. Boundary conditions in a general form of the cylindrical sandwich panel can be derived from Hamilton's principal. Using Hamilton's principle (Eq.(7)),strain-displacement relation in face-sheets (Eq.(2)) and core (Eq.(5)), compatibility condition (Eq.(6)), stresses and stresses result in the face- sheets and core, finally, equations of motion for a circular cylindrical sandwich panel can be obtained as follows:

$$\begin{aligned}
&\delta u_0^t: \\
&N^t_{xx,x} + \frac{N^t_{x\theta,\theta}}{R_t} + \frac{2}{h_c^2} M^c_{2xx,x} + \frac{C_0}{R_t} M^t_{x\theta,\theta} + \frac{4}{h_c^3} M^c_{3xx,x} + \frac{2}{R_c h_c^2} M^c_{2\theta x,\theta} + \frac{4}{R_c h_c^3} M^c_{3\theta x,\theta} - \frac{4}{h_c^2} M^{*c}_{1xz} \\
&-\frac{12}{h_c^3} M^{*c}_{2xz} = \left(I_0^t \ddot{u}_0^t + I_1^t \ddot{\psi}_x^t\right) + \left(\frac{2}{h_c^2} I_2^c + \frac{4}{h_c^3} I_3^c - \frac{8I_4^c}{h_c^4} - \frac{16I_5^c}{h_c^5}\right)\ddot{u}_0^c + \left(\frac{2I_3^c}{h_c^2} + \frac{4I_4^c}{h_c^3} - \frac{8I_5^c}{h_c^4} - \frac{16I_6^c}{h_c^5}\right)\ddot{u}_1^c \\
&+\left(\frac{4I_4^c}{h_c^4} - \frac{16I_6^c}{h_c^6}\right)\ddot{u}_0^b + \left(\frac{4I_4^c}{h_c^4} + \frac{16I_5^c}{h_c^5} + \frac{16I_6^c}{h_c^6}\right)\ddot{u}_0^t + \left(\frac{2h_b I_4^c}{h_c^4} - \frac{8h_b I_6^c}{h_c^6}\right)\ddot{\psi}_x^b + \left(-\frac{2h_t I_4^c}{h_c^4} - \frac{8h_t I_5^c}{h_c^5} - \frac{8h_t I_6^c}{h_c^6}\right)\ddot{\psi}_x^t
\end{aligned} \tag{8}$$

$$\begin{aligned}
&\delta u_0^b: \\
&N^b_{xx,x} + \frac{N^b_{x\theta,\theta}}{R_b} + \frac{C_0}{R_b} M^b_{x\theta,\theta} + \frac{2}{h_c^2} M^c_{2xx,x} - \frac{4}{h_c^3} M^c_{3xx,x} + \frac{2}{R_c h_c^2} M^c_{2\theta x,\theta} - \frac{4}{R_c h_c^3} M^c_{3\theta x,\theta} - \frac{4}{h_c^2} M^{*c}_{1xz} \\
&+\frac{12}{h_c^3} M^{*c}_{2xz} + C_0^b \frac{\partial M^b_{x\theta}}{R_b \partial \theta} = \left(I_0^b \ddot{u}_0^b + I_1^b \ddot{\psi}_x^b\right) + \left(\frac{2}{h_c^2} I_2^c - \frac{4}{h_c^3} I_3^c - \frac{8I_4^c}{h_c^4} + \frac{16I_5^c}{h_c^5}\right)\ddot{u}_0^c + \left(\frac{2I_3^c}{h_c^2} - \frac{4I_4^c}{h_c^3} - \frac{8I_5^c}{h_c^4} + \frac{16I_6^c}{h_c^5}\right)\ddot{u}_1^c \\
&+\left(\frac{4I_4^c}{h_c^4} - \frac{16I_5^c}{h_c^5} + \frac{16I_6^c}{h_c^6}\right)\ddot{u}_0^b + \left(\frac{4I_4^c}{h_c^4} - \frac{16I_6^c}{h_c^6}\right)\ddot{u}_0^t \left(\frac{2h_b I_4^c}{h_c^4} - \frac{8h_b I_5^c}{h_c^5} + \frac{8h_b I_6^c}{h_c^6}\right)\ddot{\psi}_x^b + \left(-\frac{2h_t I_4^c}{h_c^4} + \frac{8h_t I_6^c}{h_c^6}\right)\ddot{\psi}_x^t
\end{aligned} \tag{9}$$

$$\begin{aligned}
&\delta v_0^t: \\
&N^t_{x\theta,x} + \frac{1}{R_t} N^t_{\theta\theta,\theta} - \frac{C_0}{R_t} M^t_{x\theta,x} + \frac{Q^t_{\theta z}}{R_t} + \frac{2}{R_c h_c^2} M^c_{2\theta\theta,\theta} + \frac{4}{R_c h_c^3} M^c_{3\theta\theta,\theta} + \frac{2}{h_c^2} M^c_{2x\theta,x} + \frac{4}{h_c^3} M^c_{3x\theta,x} + \frac{2}{R_c h_c^2} M^c_{2\theta z} \\
&+\frac{4}{R_c h_c^3} M^c_{3\theta z} - \frac{4}{h_c^2} M^{*c}_{1\theta z} - \frac{12}{h_c^3} M^{*c}_{2\theta z} = \left(I_0^t \ddot{v}_0^t + I_1^t \ddot{\psi}_\theta^t\right) + \left(\frac{2}{h_c^2}(I_2^c + \frac{I_3^c}{R_c}) + \frac{4}{h_c^3}(I_3^c + \frac{I_4^c}{R_c}) - \frac{8I_4^c}{h_c^4} - \frac{8I_5^c}{h_c^4 R_c} - \frac{16I_5^c}{h_c^5}\right. \\
&\left.-\frac{16I_6^c}{R_c h_c^5}\right)\ddot{v}_0^c + \left(\frac{2I_3^c}{h_c^2} + \frac{4I_4^c}{h_c^3} - \frac{8I_5^c}{h_c^4} - \frac{16I_6^c}{h_c^5}\right)\ddot{v}_1^c + \left(\frac{4I_4^c}{h_c^4} - \frac{16I_6^c}{h_c^6}\right)\ddot{v}_0^b + \left(\frac{4I_4^c}{h_c^4} + \frac{16I_5^c}{h_c^5}\frac{16I_6^c}{h_c^6}\right)\ddot{v}_0^t \\
&+\left(\frac{2h_b I_4^c}{h_c^4} - \frac{8h_b I_6^c}{h_c^6}\right)\ddot{\psi}_\theta^b + \left(-\frac{2h_t I_4^c}{h_c^4} - \frac{8h_t I_5^c}{h_c^5} - \frac{8h_t I_6^c}{h_c^6}\right)\ddot{\psi}_\theta^t
\end{aligned} \tag{10}$$

δv_0^b :

$$N_{x\theta,x}^b+\frac{1}{R_b}N_{\theta\theta,\theta}^b-C_0M_{x\theta,x}^b+\frac{Q_{\theta z}^b}{R_b}+\frac{2}{R_ch_c^2}M_{2\theta\theta,\theta}^c-\frac{4}{R_ch_c^3}M_{3\theta\theta,\theta}^c+\frac{2}{h_c^2}M_{2x\theta,x}^c-\frac{4}{h_c^3}M_{3x\theta,x}^c+\frac{2}{R_ch_c^2}M_{2\theta z}^c$$
$$-\frac{4}{R_ch_c^3}M_{3\theta z}^c-\frac{4}{h_c^2}M_{1\theta z}^{*c}+\frac{12}{h_c^3}M_{2\theta z}^{*c}=\left(I_0^b\ddot{v}_0^b+I_1^b\ddot{\psi}_\theta^b\right)+(\frac{2}{h_c^2}(I_2^c+\frac{I_3^c}{R_c})-\frac{4}{h_c^3}(I_3^c+\frac{I_4^c}{R_c})-\frac{8I_4^c}{h_c^4}-\frac{8I_5^c}{h_c^4R_c}$$
$$+\frac{16I_5^c}{h_c^5}+\frac{16I_6^c}{R_ch_c^5})\ddot{v}_0^c+\left(\frac{2I_3^c}{h_c^2}-\frac{4I_4^c}{h_c^3}-\frac{8I_5^c}{h_c^4}+\frac{16I_6^c}{h_c^5}\right)\ddot{v}_1^c+\left(\frac{4I_4^c}{h_c^4}-\frac{16I_5^c}{h_c^5}+\frac{16I_6^c}{h_c^6}\right)\ddot{v}_0^b+\left(\frac{4I_4^c}{h_c^4}-\frac{16I_6^c}{h_c^6}\right)\ddot{v}_0^t+$$
$$\left(\frac{2h_bI_4^c}{h_c^4}-\frac{8h_bI_5^c}{h_c^5}+\frac{8h_bI_6^c}{h_c^6}\right)\ddot{\psi}_\theta^b$$
$$+\left(-\frac{2h_tI_4^c}{h_c^4}+\frac{8h_tI_6^c}{h_c^6}\right)\ddot{\psi}_\theta^t \tag{11}$$

δw_0^t :

$$Q_{xz,x}^t+\frac{1}{R_t}Q_{\theta z,\theta}^t-\frac{N_{\theta\theta}^t}{R_t}-\frac{R_z^c}{h_c}-\frac{4}{h_c^2}M_z^c-\frac{1}{R_ch_c}M_{1\theta\theta}^c-\frac{2}{R_ch_c^2}M_{2\theta\theta}^c+\frac{1}{h_c}M_{1xz,x}^c+\frac{2}{h_c^2}M_{2xz,x}^c+\frac{1}{R_ch_c}M_{1\theta z,\theta}^c+\frac{2}{R_ch_c^2}M_{2\theta z,\theta}^c$$
$$-(1+\frac{h_t}{2R_{ty}})q_t=\left(I_0^t\ddot{w}_0^t\right)+\left(\frac{I_1^c}{h_c}+\frac{2I_2^c}{h_c^2}-\frac{4I_3^c}{h_c^3}-\frac{8I_4^c}{h_c^4}\right)\ddot{w}_0^c+\left(\frac{I_2^c}{h_c^2}+\frac{4I_3^c}{h_c^3}+\frac{4I_4^c}{h_c^4}\right)\ddot{w}_0^t+\left(-\frac{I_2^c}{h_c^2}+\frac{4I_4^c}{h_c^4}\right)\ddot{w}_0^b \tag{12}$$

δw_0^b :

$$Q_{xz,x}^b+\frac{1}{R_b}Q_{\theta z,\theta}^b-\frac{N_{\theta\theta}^b}{R_b}+\frac{R_z^c}{h_c}-\frac{4}{h_c^2}M_z^c+\frac{1}{R_ch_c}M_{1\theta\theta}^c-\frac{2}{R_ch_c^2}M_{2\theta\theta}^c-\frac{1}{h_c}M_{1xz,x}^c+\frac{2}{h_c^2}M_{2xz,x}^c$$
$$-\frac{1}{h_c}M_{1\theta z,\theta}^c+\frac{2}{h_c^2}M_{2\theta z,\theta}^c+(1-\frac{h_b}{2R_{by}})q_b \tag{13}$$
$$=\left(I_0^b\ddot{w}_0^b\right)+\left(-\frac{I_1^c}{h_c}+\frac{2I_2^c}{h_c^2}+\frac{4I_3^c}{h_c^3}-\frac{8I_4^c}{h_c^4}\right)\ddot{w}_0^c+\left(\frac{I_2^c}{h_c^2}-\frac{4I_3^c}{h_c^3}+\frac{4I_4^c}{h_c^4}\right)\ddot{w}_0^b+\left(-\frac{I_2^c}{h_c^2}+\frac{4I_4^c}{h_c^4}\right)\ddot{w}_0^t$$

$\delta\psi_x^t$:

$$(M_{xx,x}^t+\frac{1}{R_t}M_{x\theta,\theta}^t-Q_{xz}^t-\frac{h_t}{h_c^2}M_{2xx,x}^c-\frac{2h_t}{h_c^3}M_{3xx,x}^c-\frac{h_t}{R_ch_c^2}M_{2\theta x,\theta}^c-\frac{2h_t}{R_ch_c^3}M_{3\theta x,\theta}^c+\frac{2h_t}{h_c^2}M_{1xz}^{*c}+\frac{6h_t}{h_c^3}M_{2xz}^{*c})$$
$$=\left(I_1^t\ddot{u}_0^t+I_2^t\ddot{\psi}_x^t\right)+(-\frac{h_t}{h_c^2}I_2^c-\frac{2h_t}{h_c^3}I_3^c+\frac{4h_tI_4^c}{h_c^4}+\frac{8h_tI_5^c}{h_c^5})\ddot{u}_0^c+(-\frac{h_tI_3^c}{h_c^2}-\frac{2h_tI_4^c}{h_c^3}+\frac{4h_tI_5^c}{h_c^4}+\frac{8h_tI_6^c}{h_c^5})\ddot{u}_1^c$$
$$+(-\frac{2h_bI_4^c}{h_c^4}+\frac{8h_bI_6^c}{h_c^6})\ddot{u}_0^b+\left(-\frac{2h_tI_4^c}{h_c^4}+\frac{8h_tI_5^c}{h_c^5}-\frac{8h_tI_6^c}{h_c^6}\right)\ddot{u}_0^t+\left(-\frac{h_th_bI_4^c}{h_c^4}+\frac{4h_th_bI_6^c}{h_c^6}\right)\ddot{\psi}_x^b+$$
$$\left(\frac{h_t^2I_4^c}{h_c^4}+\frac{4h_t^2I_5^c}{h_c^5}+\frac{4h_t^2I_6^c}{h_c^6}\right)\ddot{\psi}_x^t \tag{14}$$

$\delta\psi_x^b$:

$$M^b_{xx,x}+\frac{1}{R_b}M^b_{x\theta,\theta}-Q^b_{xz}+\frac{h_b}{h_c^2}M^c_{2xx,x}-\frac{2h_b}{h_c^3}M^c_{3xx,x}-\frac{h_b}{R_ch_c^2}M^c_{2\theta x,\theta}-\frac{2h_b}{R_ch_c^3}M^c_{3\theta x,\theta}-\frac{2h_b}{h_c^2}M^{*c}_{1xz}+\frac{6h_b}{h_c^3}M^{*c}_{2xz}$$
$$=\left(I_1^b\ddot{u}_0^b+I_2^b\ddot{\psi}_x^b\right)+(\frac{h_b}{h_c^2}I_2^c-\frac{2h_b}{h_c^3}I_3^c-\frac{4h_bI_4^c}{h_c^4}+\frac{8h_bI_5^c}{h_c^5})\ddot{u}_0^c+(\frac{h_bI_3^c}{h_c^2}-\frac{2h_bI_4^c}{h_c^3}-\frac{4h_bI_5^c}{h_c^4}+\frac{8h_bI_6^c}{h_c^5})\ddot{u}_1^c+(\frac{2h_bI_4^c}{h_c^4}- \tag{15}$$
$$\frac{8h_bI_5^c}{h_c^5}+\frac{8h_bI_6^c}{h_c^6})\ddot{u}_0^b+\left(\frac{2h_tI_4^c}{h_c^4}-\frac{8h_tI_6^c}{h_c^6}\right)\ddot{u}_0^t+\left(\frac{h_b^2I_4^c}{h_c^4}-\frac{4h_b^2I_5^c}{h_c^5}+\frac{4h_b^2I_6^c}{h_c^6}\right)\ddot{\psi}_x^b+\left(-\frac{h_th_bI_4^c}{h_c^4}+\frac{4h_th_bI_6^c}{h_c^6}\right)\ddot{\psi}_x^t$$

$\delta\psi_\theta^t$:

$$(M^t_{x\theta,x}+\frac{1}{R_t}M^t_{\theta\theta,\theta}-Q^t_{\theta z}-\frac{h_t}{R_ch_c^2}M^c_{2\theta\theta,\theta}-\frac{2h_t}{R_ch_c^3}M^c_{3\theta\theta,\theta}-\frac{h_t}{h_c^2}M^c_{2x\theta,x}-\frac{2h_t}{h_c^3}M^c_{3x\theta,x}+\frac{2h_t}{h_c^2}M^{*c}_{1\theta z}+$$
$$\frac{6h_t}{h_c^3}M^{*c}_{2\theta z})=\left(I_1^t\ddot{v}_0^t+I_2^t\ddot{\psi}_\theta^t\right)+(-\frac{h_t}{h_c^2}(I_2^c+\frac{I_3^c}{R_c})-\frac{2h_t}{h_c^3}(I_3^c+\frac{I_4^c}{R_c})+\frac{4h_tI_4^c}{h_c^4}+\frac{4h_tI_5^c}{R_ch_c^4}+\frac{8h_tI_5^c}{h_c^5}+\frac{8h_tI_6^c}{R_ch_c^5})\ddot{v}_0^c \tag{16}$$
$$+\left(-\frac{h_tI_3^c}{h_c^2}-\frac{2h_tI_4^c}{h_c^3}+\frac{4h_tI_5^c}{h_c^4}+\frac{8h_tI_6^c}{h_c^5}\right)\ddot{v}_1^c+\left(-\frac{2h_tI_4^c}{h_c^4}+\frac{8h_tI_6^c}{h_c^6}\right)\ddot{v}_0^b+\left(-\frac{2h_tI_4^c}{h_c^4}+\frac{8h_tI_5^c}{h_c^5}-\frac{8h_tI_6^c}{h_c^6}\right)\ddot{v}_0^t$$
$$+\left(-\frac{h_th_bI_4^c}{h_c^4}+\frac{4h_th_bI_6^c}{h_c^6}\right)\ddot{\psi}_\theta^b+\left(\frac{h_t^2I_4^c}{h_c^4}+\frac{4h_t^2I_5^c}{h_c^5}+\frac{4h_t^2I_6^c}{h_c^6}\right)\ddot{\psi}_\theta^t$$

$\delta\psi_\theta^b$:

$$(M^b_{x\theta,x}+\frac{1}{R_b}M^b_{\theta\theta,\theta}-Q^b_{\theta z}+\frac{h_b}{R_ch_c^2}M^c_{2\theta\theta,\theta}-\frac{2h_b}{R_ch_c^3}M^c_{3\theta\theta,\theta}+\frac{h_b}{h_c^2}M^c_{2x\theta,x}-\frac{2h_b}{h_c^3}M^c_{3x\theta,x}-\frac{h_b}{R_ch_c^2}M^c_{2\theta z}-$$
$$\frac{2h_b}{R_ch_c^2}M^c_{3\theta z}-\frac{2h_b}{h_c^2}M^{*c}_{1\theta z}+\frac{6h_b}{h_c^3}M^{*c}_{2\theta z})=\left(I_1^b\ddot{v}_0^b+I_2^b\ddot{\psi}_\theta^b\right)+(\frac{h_b}{h_c^2}(I_2^c+\frac{I_3^c}{R_c})-\frac{2h_b}{h_c^3}(I_3^c+\frac{I_4^c}{R_c})-\frac{4h_bI_4^c}{h_c^4}$$
$$-\frac{4h_bI_5^c}{R_ch_c^4}+\frac{8h_bI_5^c}{h_c^5}+\frac{8h_bI_6^c}{R_ch_c^5})\ddot{v}_0^c+\left(\frac{h_bI_3^c}{h_c^2}-\frac{2h_bI_4^c}{h_c^3}-\frac{4h_bI_5^c}{h_c^4}+\frac{8h_bI_6^c}{h_c^5}\right)\ddot{v}_1^c+\left(\frac{2h_bI_4^c}{h_c^4}-\frac{8h_bI_5^c}{h_c^5}+\frac{8h_bI_6^c}{h_c^6}\right)\ddot{v}_0^b \tag{17}$$
$$+\left(\frac{2h_tI_4^c}{h_c^4}-\frac{8h_tI_6^c}{h_c^6}\right)\ddot{v}_0^t+\left(\frac{h_b^2I_4^c}{h_c^4}-\frac{4h_b^2I_5^c}{h_c^5}+\frac{4h_b^2I_6^c}{h_c^6}\right)\ddot{\psi}_\theta^b+\left(-\frac{h_th_bI_4^c}{h_c^4}+\frac{4h_th_bI_6^c}{h_c^6}\right)\ddot{\psi}_\theta^t$$

δu_0^c :

$$(N^c_{xx,x}+\frac{1}{R_c}N^c_{\theta x,\theta}-\frac{4}{h_c^2}M^c_{2xx,x}-\frac{4}{R_ch_c^2}M^c_{2\theta x,\theta}+\frac{8}{h_c^2}M^{*c}_{1xz})=\left(I_0^c-\frac{8}{h_c^2}I_2^c+\frac{16I_4^c}{h_c^4}\right)\ddot{u}_0^c+(I_1^c-\frac{8I_3^c}{h_c^2}$$
$$+\frac{16I_5^c}{h_c^4})\ddot{u}_1^c+\left(\frac{2}{h_c^2}I_2^c-\frac{4}{h_c^3}I_3^c-\frac{8I_4^c}{h_c^4}+\frac{16I_5^c}{h_c^5}\right)\ddot{u}_0^b+(\frac{2}{h_c^2}I_2^c+\frac{4}{h_c^3}I_3^c-\frac{8I_4^c}{h_c^4}-\frac{16I_5^c}{h_c^5})\ddot{u}_0^t+(\frac{h_b}{h_c^2}I_2^c-\frac{2h_b}{h_c^3}I_3^c- \tag{18}$$
$$\frac{4h_bI_4^c}{h_c^4}+\frac{8h_bI_5^c}{h_c^5})\ddot{\psi}_x^b+\left(-\frac{h_t}{h_c^2}I_2^c-\frac{2h_t}{h_c^3}I_3^c+\frac{4h_tI_4^c}{h_c^4}+\frac{8h_tI_5^c}{h_c^5}\right)\ddot{\psi}_x^t$$

δu_1^c :

$$M^c_{1xx,x} - N^{*c}_{xz} - \frac{4}{h_c^2}M^c_{3xx,x} + \frac{1}{R_c}M^c_{1\theta x,\theta} - \frac{4}{R_c h_c^2}M^c_{3\theta x,\theta} + \frac{12}{h_c^2}M^{*c}_{2xz} = \left(I_1^c - \frac{8I_3^c}{h_c^2} + \frac{16I_5^c}{h_c^4}\right)\ddot{u}_0^c$$
$$+\left(I_2^c - \frac{8I_4^c}{h_c^2} + \frac{16I_6^c}{h_c^4}\right)\ddot{u}_1^c + \left(\frac{2I_3^c}{h_c^2} - \frac{4I_4^c}{h_c^3} - \frac{8I_5^c}{h_c^4} + \frac{16I_6^c}{h_c^5}\right)\ddot{u}_0^b + \left(\frac{2I_3^c}{h_c^2} + \frac{4I_4^c}{h_c^3} - \frac{8I_5^c}{h_c^4} - \frac{16I_6^c}{h_c^5}\right)\ddot{u}_0^t \quad (19)$$
$$+\left(\frac{h_b I_3^c}{h_c^2} - \frac{2h_b I_4^c}{h_c^3} - \frac{4h_b I_5^c}{h_c^4} + \frac{8h_b I_6^c}{h_c^5}\right)\ddot{\psi}_x^b + \left(-\frac{h_t I_3^c}{h_c^2} - \frac{2h_t I_4^c}{h_c^3} + \frac{4h_t I_5^c}{h_c^4} + \frac{8h_t I_6^c}{h_c^5}\right)\ddot{\psi}_x^t$$

δv_0^c :

$$\frac{1}{R_c}N^c_{\theta\theta,\theta} + N^c_{x\theta,x} - \frac{4}{R_c h_c^2}M^c_{2\theta\theta,\theta} - \frac{4}{R_c^2 h_c^2}M^c_{3\theta\theta,\theta} + \frac{1}{R_c}M^c_{1x\theta,x} - \frac{4}{h_c^2}M^c_{2x\theta,x} - \frac{4}{R_c h_c^2}M^c_{3x\theta,x} + \frac{1}{R_c}N^c_{\theta z} -$$
$$\frac{4}{R_c h_c^2}M^c_{2\theta z} - \frac{4}{R_c^2 h_c^2}M^c_{3\theta z} + \frac{8}{h_c^2}M^{*c}_{1\theta z} + \frac{12}{R_c h_c^2}M^{*c}_{2\theta z} - \frac{1}{R_c}N^{*c}_{\theta z} = \left(I_0^c + \frac{I_2^c}{R_c^2} + \frac{2I_1^c}{R_c} - \frac{8}{h_c^2}\left(I_2^c + \frac{I_3^c}{R_c}\right)\right.$$
$$\left.-\frac{8}{h_c^2 R_c}\left(I_3^c + \frac{I_4^c}{R_c}\right) + \frac{16I_4^c}{h_c^4} + \frac{32I_5^c}{R_c h_c^4} + \frac{16I_6^c}{R_c^2 h_c^4}\right)\ddot{v}_0^c + \left(I_1^c + \frac{I_2^c}{R_c} - \frac{8I_3^c}{h_c^2} - \frac{8I_4^c}{h_c^2 R_c} + \frac{16I_5^c}{h_c^4} + \frac{16I_6^c}{R_c h_c^4}\right)\ddot{v}_1^c + \quad (20)$$
$$\left(\frac{2}{h_c^2}\left(I_2^c + \frac{I_3^c}{R_c}\right) - \frac{4}{h_c^3}\left(I_3^c + \frac{I_4^c}{R_c}\right) - \frac{8I_4^c}{h_c^4} + \frac{16I_5^c}{h_c^5} - \frac{8I_5^c}{R_c h_c^4} + \frac{16I_6^c}{R_c h_c^5}\right)\ddot{v}_0^b + \left(\frac{2}{h_c^2}\left(I_2^c + \frac{I_3^c}{R_c}\right) + \frac{4}{h_c^3}\left(I_3^c + \frac{I_4^c}{R_c}\right)\right.$$
$$\left.-\frac{8I_4^c}{h_c^4} - \frac{16I_5^c}{h_c^5} - \frac{8I_5^c}{R_c h_c^4} - \frac{16I_6^c}{R_c h_c^5}\right)\ddot{v}_0^t + \left(\frac{h_b}{h_c^2}\left(I_2^c + \frac{I_3^c}{R_c}\right) - \frac{2h_b}{h_c^3}\left(I_3^c + \frac{I_4^c}{R_c}\right) - \frac{4h_b I_4^c}{h_c^4} + \frac{8h_b I_5^c}{h_c^5} - \frac{4h_c h_b I_5^c}{R_c h_c^5}\right)\ddot{\psi}_\theta^b$$
$$+\left(-\frac{h_t}{h_c^2}\left(I_2^c + \frac{I_3^c}{R_c}\right) - \frac{2h_t}{h_c^3}\left(I_3^c + \frac{I_4^c}{R_c}\right) + \frac{4h_t I_4^c}{h_c^4} + \frac{8h_t I_5^c}{h_c^5} + \frac{4h_c h_t I_5^c}{R_c h_c^5} + \frac{8h_c h_t I_6^c}{R_c h_c^6}\right)\ddot{\psi}_x^t$$

δv_1^c :

$$\left(\frac{1}{R_c}M^c_{1\theta\theta,\theta} - N^{*c}_{\theta z} - \frac{4}{R_c h_c^2}M^c_{3\theta\theta,\theta} + M^c_{1x\theta,x} - \frac{4}{h_c^2}M^c_{3x\theta,x} + \frac{1}{R_c}M^c_{1\theta z} - \frac{4}{R_c h_c^2}M^c_{3\theta z} + \frac{12}{h_c^2}M^{*c}_{2\theta z}\right)$$
$$= \left(I_1^c + \frac{I_2^c}{R_c} - \frac{8I_3^c}{h_c^2} - \frac{8I_4^c}{h_c^2 R_c} + \frac{16I_5^c}{h_c^4} + \frac{16I_6^c}{R_c h_c^4}\right)\ddot{v}_0^c + \left(I_2^c - \frac{8I_4^c}{h_c^2} + \frac{16I_6^c}{h_c^4}\right)\ddot{v}_1^c + \left(\frac{2I_3^c}{h_c^2} - \frac{4I_4^c}{h_c^3} - \frac{8I_5^c}{h_c^4} + \right. \quad (21)$$
$$\left.\frac{16I_6^c}{h_c^5}\right)\ddot{v}_0^b + \left(\frac{2I_3^c}{h_c^2} + \frac{4I_4^c}{h_c^3} - \frac{8I_5^c}{h_c^4} - \frac{16I_6^c}{h_c^5}\right)\ddot{v}_0^t + \left(\frac{h_b I_3^c}{h_c^2} - \frac{2h_b I_4^c}{h_c^3} - \frac{4h_b I_5^c}{h_c^4} + \frac{8h_b I_6^c}{h_c^5}\right)\ddot{\psi}_\theta^b +$$
$$\left(-\frac{h_t I_3^c}{h_c^2} - \frac{2h_t I_4^c}{h_c^3} + \frac{4h_t I_5^c}{h_c^4} + \frac{8h_t I_6^c}{h_c^5}\right)\ddot{\psi}_\theta^t$$

δw_o^c :

$$N^c_{xz,x} + \frac{1}{R_c}N^c_{\theta z,\theta} + \frac{8}{h_c^2}M^c_z - \frac{1}{R_c}N^c_{\theta\theta} + \frac{4}{R_c h_c^2}M^c_{2\theta\theta} - \frac{4}{h_c^2}M^c_{2xz,x} - \frac{4}{R_c h_c^2}M^c_{2\theta z,\theta} = \left(I_0^c - \frac{8I_2^c}{h_c^2}\right. \quad (22)$$
$$\left.+\frac{16I_4^c}{h_c^4}\right)\ddot{w}_0^c + \left(\frac{I_1^c}{h_c} + \frac{2I_2^c}{h_c^2} - \frac{4I_3^c}{h_c^3} - \frac{8I_4^c}{h_c^4}\right)\ddot{w}_0^t + \left(-\frac{I_1^c}{h_c} + \frac{2I_2^c}{h_c^2} + \frac{4I_3^c}{h_c^3} - \frac{8I_4^c}{h_c^4}\right)\ddot{w}_0^b$$

$$I_m^i = \int_{-\frac{h_i}{2}}^{\frac{h_i}{2}} \left(z_i^m \rho_i\right) dz_i \ , \quad I_n^c = \int_{-\frac{h_c}{2}}^{\frac{h_c}{2}} \rho_c z_c^n (1+z_c/R_c)\, dz_c \ , \quad C_0^i = \frac{1}{2}\left(\frac{1}{R_{xi}} - \frac{1}{R_{yi}}\right); \ i = t,b \ ; m = 1,2,3; \ n = 0,1,...,6 \tag{23}$$

where:

$$\begin{Bmatrix} N_{xx}^c \\ N_{\theta\theta}^c \\ N_{x\theta}^c \\ N_{\theta x}^c \end{Bmatrix} = \int_{-h_c/2}^{h_c/2} \begin{Bmatrix} \sigma_{xx}^c (1+\frac{z_c}{R_c}) \\ \sigma_{\theta\theta}^c \\ \sigma_{x\theta}^c (1+\frac{z_c}{R_c}) \\ \sigma_{x\theta}^c \end{Bmatrix} dz_c, \qquad \begin{Bmatrix} M_{nxx}^c \\ M_{n\theta\theta}^c \\ M_{nx\theta}^c \\ M_{n\theta x}^c \end{Bmatrix} = \int_{-h_c/2}^{h_c/2} z_c^n \begin{Bmatrix} \sigma_{xx}^c (1+\frac{z_c}{R_c}) \\ \sigma_{\theta\theta}^c \\ \sigma_{x\theta}^c (1+\frac{z_c}{R_c}) \\ \sigma_{x\theta}^c \end{Bmatrix} dz_c$$

$$\begin{Bmatrix} N_{xz}^c \\ N_{\theta z}^c \\ M_{nxz}^c \\ M_{n\theta z}^c \end{Bmatrix} = \int_{-h_c/2}^{h_c/2} \begin{Bmatrix} \sigma_{xz}^c (1+\frac{z_c}{R_c}) \\ \sigma_{\theta z}^c \\ z_c^n \sigma_{xz}^c (1+\frac{z_c}{R_c}) \\ z_c^n \sigma_{\theta z}^c \end{Bmatrix} dz_c, \qquad \begin{Bmatrix} N_{xz}^{*c} \\ N_{\theta z}^{*c} \\ M_{nxz}^{*c} \\ M_{n\theta z}^{*c} \end{Bmatrix} = \int_{-h_c/2}^{h_c/2} \begin{Bmatrix} \sigma_{xz}^c \\ \sigma_{\theta z}^c \\ z_c^n \sigma_{xz}^c \\ z_c^n \sigma_{\theta z}^c \end{Bmatrix} (1+\frac{z_c}{R_{yc}}) dz_c$$

$$\left\{R_z^c, M_z^c\right\} = \int_{-h_c/2}^{h_c/2} (1, z_c)\, \sigma_{zz}^c (1+\frac{z_c}{R_c}) dz_c, \tag{24}$$

$$\begin{Bmatrix} N_{xx}^i \\ N_{\theta\theta}^i \\ N_{x\theta}^i \\ N_{\theta x}^i \end{Bmatrix} = \int_{-h_i/2}^{h_i/2} \begin{Bmatrix} \sigma_{xx}^i \\ \sigma_{\theta\theta}^i \\ \sigma_{xv}^i \\ \sigma_{x\theta}^i \end{Bmatrix} dz_i, \qquad \begin{Bmatrix} M_{xx}^i \\ M_{\theta\theta}^i \\ M_{x\theta}^i \\ M_{\theta x}^i \end{Bmatrix} = \int_{-h_i/2}^{h_i/2} z_i \begin{Bmatrix} \sigma_{xx}^i \\ \sigma_{\theta\theta}^i \\ \sigma_{x\theta}^i \\ \sigma_{x\theta}^i \end{Bmatrix} dz_i$$

$$\begin{Bmatrix} Q_{xz}^i \\ Q_{\theta z}^i \end{Bmatrix} = k_s \int_{-h_i/2}^{h_i/2} \begin{Bmatrix} \sigma_{xz}^i \\ \sigma_{\theta z}^i \end{Bmatrix} dz_i, \qquad ; i = t,b \text{ and } n = 1,2,3$$

Using stress-strain relations in orthotropic face-sheets, the governing equations in terms of the displacement field of upper and lower face-sheets as well as the equation related to the core are expressed.

3 IMPACT FORCE MODELS

Consider a circular cylindrical composite sandwich panel(Figure 3.1a) which is subjected to N number of strikes of the impactor masses at points with the coordinates (x_1 ,y_1), (x_2 ,y_2), and (x_n ,y_n). Masses and velocities of the impactors are (M_1, V_1), (M_2, V_2), and (M_n, V_n), respectively. In the obtained equations of motion, the contact load q_j(j = t, b) is assumed to be represented by series expansion as follows:

$$q_t(x,\theta,t)=\sum_{m=1}^{\infty}\sum_{n=0}^{\infty}[\sum_{i=1}^{N}q_{mn}^{i}(t)]\sin(\alpha_m x)\cos(n\theta) \tag{25}$$

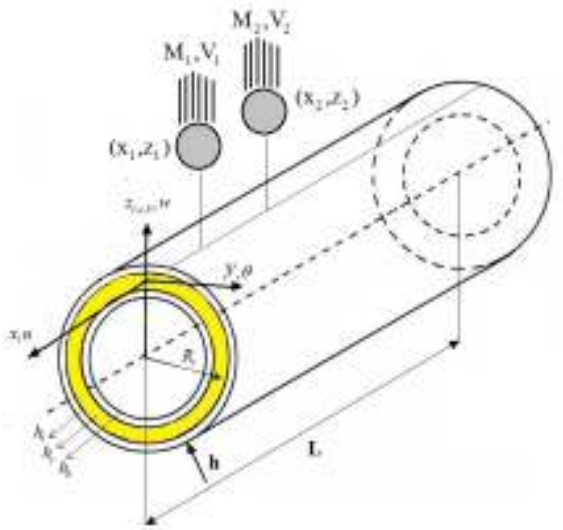

Figure 3.1a: A circular cylindrical sandwich panel with laminated face-sheets along with the orthogonal curvilinear coordinates and dimensions of the panel and impactors.

Fourier coefficients q_{mn}^{i}, (i=1,2,...,N) for concentrated contact loads $F_c^i(t)$ located at points (x_i,θ_i) of the top face-sheets become:

$$\begin{cases} q_{m0}^{i}(t)=\dfrac{F_c^i(t)}{\pi LR}\sin(\alpha_m x_i) & if \quad n=0 \\ q_{mn}^{i}(t)=\dfrac{2F_c^i(t)}{\pi LR}\sin(\alpha_m x_i)\cos(n\theta_i) & if \quad n>0 \end{cases} \qquad \alpha_m=\frac{m\pi}{a} \tag{26}$$

L is the length of circular cylindrical panel and i is the superscript and denotes the "i"th impact (i=1, 2, 3,....N). The contact force, $F_c^i(t)$, will be calculated from spring-mass model with two degrees of freedom and complete models. Similarly, for uniform dynamic contact loads $F_c^i(t)$ distributed on patches with length $2L_1^i$ and width $2L_2^i$, the applied load is assumed to be only in the radial direction over a small rectangular area ($2L_2^i \times 2L_1^i$). Regarding Figure 3.1b, the area of applied load is variable and the center of this area can be everywhere on the top face-sheet as:

$$\begin{aligned} &x_{i2}-x_{i1}=2l_2^i \ \text{ and } \ R(\psi_{i2}-\psi_{i1})=2l_1^i \\ &x_{iL}=\frac{x_{i2}+x_{i1}}{2} \ \text{ and } \ \varphi_{iL}=\frac{\psi_{i2}+\psi_{i1}}{2} \end{aligned} \tag{27}$$

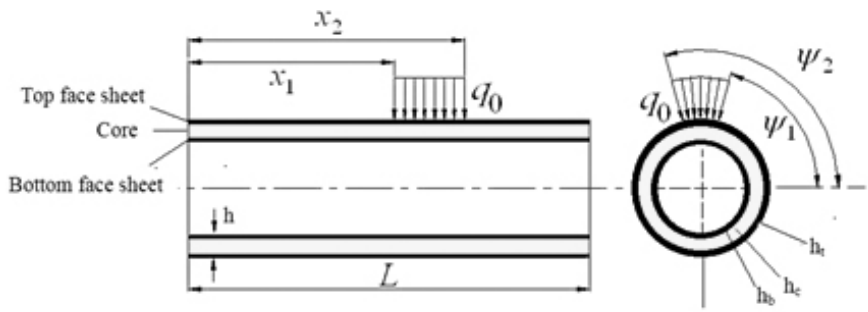

Figure 3.1b: Load applied laterally on a small rectangular area on the top or bottom face-sheet of a circular cylindrical sandwich panel.

where x_{iL} and φ_{iL} are coordinates indicating the center point of the applied load area. So, the constant Fourier coefficients q_{mn}^{i} can be determined as follows:

$$\begin{cases} q_{mn}^{i}(t) = \dfrac{F_c^i(t)}{m\pi^2}[\cos(\alpha_m x_{2i}) - \cos(\alpha_m x_{1i})](\psi_{2i} - \psi_{1i}) & if \quad n = 0 \\ q_{mn}^{i}(t) = \dfrac{2F_c^i(t)}{mn\pi^2}[\cos(\alpha_m x_{2i}) - \cos(\alpha_m x_{1i})](\sin(n\psi_{2i}) - \sin(n\psi_{1i})) & if \quad n > 0 \end{cases} \tag{28}$$

In this paper, it was assumed that the vibration of the projectile can be negligible [6].To predict the impact forces, different methods such as finite element code, spring-mass system, and Hertz's perfect model could be used. In the modified Hertz's contact law, the contact force, $F_c^i(t)$, between the "i"th impactor and the impacted face-sheet during the impact can be usually approximated and calculated according to the non-linear power law of the form in (2006):

$$F_c^i(t) = K_c^i(\alpha^i)^n \tag{29}$$

In Hertzian indentation, n=1.5 in all the impactors (1996). Contact stiffness K_c^i (i=1, 2... N) can be evaluated by the contact stiffness for a half space (1995). Indentation α^i is the relative indentation between the impactor and the impacted top face–sheet of the panel which is defined as:

$$\alpha^i = w_j^i - w_0^k(x_i, y_i) \quad ; \quad k = t \text{ or/and } b \tag{30}$$

where w_j^i denotes the displacement of the "i"th impactor and w_0^k is the transverse displacement of the impacted surface at the impact location (x_i, y_i).For an elastic spherical impactor in contact with an isotropic elastic half-plane, Timoshenko and Goodier (1951) presented a relation between the "i"th contact radius $R_{contact}^i$, applied load $F_c^i(t)$, (i = 1, 2, . . . N), impactor radius R^i , and E Malekzadeh et al., (2006).

$$R^i_{\text{contact}}(t) = 0.909.(\frac{F^i_c(t).R^i}{E})^{\frac{1}{3}} \tag{31}$$

In this paper, it was assumed that $l^i_1 = l^i_2 = 2R^i_{\text{contact}}(t)$ (Eq.29) can be calculated using Eq. (30). Equation of motion for the "i"th impactor can be written as:

$$M^i_I \ddot{w}^i_j + F^i(t) = 0 \;\Rightarrow\; w^i_j(t=0) = 0 \quad , \quad \dot{w}^i_j(t=0) = V^i_0 \tag{32}$$

Where M^i_I is the mass of the "i"th impactor, w^i_j is displacement of the "i"th impactor, and $F^i(t)$ are the contact forces between the impactors and the target structure. The impact solution for a circular sandwich panel with simply supported boundary conditions (SS) at top and bottom face-sheets is assumed to be in the following form:

$$\begin{bmatrix} u^j_0(x,\theta,t) \\ v^j_0(x,\theta,t) \\ w^j_0(x,\theta,t) \\ \psi^j_x(x,\theta,t) \\ \psi^j_\theta(x,\theta,t) \\ u^c_k(x,\theta,t) \\ v^c_k(x,\theta,t) \\ w^c_l(x,\theta,t) \end{bmatrix} = \sum_{n=0}^{\infty}\sum_{m=1}^{\infty} \begin{bmatrix} U^j_{0mn}(t)\cos(\alpha_m x)\cos(n\theta) \\ V^j_{0mn}(t)\sin(\alpha_m x)\sin(n\theta) \\ W^j_{0mn}(t)\sin(\alpha_m x)\cos(n\theta) \\ \Psi^j_{xmn}(t)\cos(\alpha_m x)\cos(n\theta) \\ \Psi^j_{\theta mn}(t)\sin(\alpha_m x)\sin(n\theta) \\ U^c_{kmn}(t)\cos(\alpha_m x)\cos(n\theta) \\ V^c_{kmn}(t)\sin(\alpha_m x)\sin(n\theta) \\ W^c_{lmn}(t)\sin(\alpha_m x)\cos(n\theta) \end{bmatrix}, \text{ (k=0,1,2,3), (l=0,1,2)} \tag{33}$$

The above double Fourier series functions can satisfy some boundary conditions for a cylindrical circular composite sandwich panel simply supported on all the edges. However, when all edges are clamped, only the function $cos\alpha_m x$ in the above series expansions must be replaced with $sin\alpha_m x$. In Eq. (31), $U^j_{0mn}, V^j_{0mn}, W^j_{0mn}, \Psi^j_{xmn}, \Psi^j_{\theta mn}, U^c_{kmn}, V^c_{kmn}, W^c_{lmn}$ are Fourier coefficients that are time-dependent unknowns, m and n are the half wave numbers along x and θ directions, respectively, and $j = t, b$, where t and b refer to the top and bottom face-sheets. By substituting stress results of cylindrical circular composite sandwich panel, compatibility conditions, and displacement field in the governing equations and then applying the Galerkin method, the governing equations are reduced to the following system of coupled ordinary differential equations:

$$\begin{aligned} &[M]\{\ddot{c}\} + [K]\{c\} = \{Q\} \\ &M^i_I \ddot{w}^i_j + F^i(t) = 0 \;\Rightarrow\; w^i_j(t=0) = 0 \quad , \quad \dot{w}^i_j(t=0) = V^i_0 \\ &F^i_c(t) = K^i_c(\alpha^i)^n \quad \Rightarrow \quad \alpha^i = w^i_j - w^k_0(x_i, y_i) \end{aligned} \tag{34}$$

Where $[M]$ is the (10 nm) ×(10 mn) square symmetric mass matrix, $[K]$ is (10 nm) ×(10 mn) square symmetric stiffness matrix, and $\{Q\}$ is the (10 nm) ×1 vector of impact forces. These differential equations can be solved by Runge-Kutta numerical method using the ODE tools of

MATLAB-7.0 software. Another method for calculating impact on cylindrical sandwich panels is modified spring-mass system with two degrees of freedom (TDOF).The spring-mass system for any impactor includes two springs and two masses. In this model, impactors are shown by masses $M_I^i (i = 1, 2, .., N)$, target structure is given by effective mass M_{eff}^s, indentation of impactors in the target structure is demonstrated by springs with stiffness K_c^i (i=1,2,...,N), and transverse deflection of impacted structure at point (x_i, y_i) are shown by springs with stiffness K_g^i (Figure 3.2).

K_g^i and M_{eff}^s are defined as (Swanson, 1992):

$$K_g^i = \frac{1}{\delta_1^i} \quad , \quad \delta_1^i = w_0^j(x_i, y_i) \; ; \; j = t \text{ or/and } b \tag{35}$$

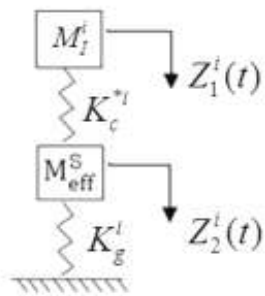

Figure 3.2: Linearized spring-mass model (Swanson, 1992).

In which δ_I^i and ω_f are displacement of the target structure and the lowest natural frequency of structure, respectively. The contact deformation between target structure and the "i"th impactor is defined as:

$$\delta^i(t) = Z_1^i(t) - Z_2^i(t) \tag{36}$$

Using the Hertz's contact law, the impact force for the "i"th impactor can be written as (1981):

$$F^i(t) = K_c^i \delta^{n_i} \tag{37}$$

In the present model, the linear form of modified Hertz's law is used. Therefore, to obtain the linearized contact deformation or contact force between the "i"th impactor and "i"th impacted structure point, the linearized contact stiffness K_c^{*I} is used. Then:

$$F_c^i = K_c^{*i}[Z_2^i(t) - Z_1^i(t)] \tag{38}$$

Using the governing equations of motion on spring-mass system in Figure 3.2, Choi's linearized form (2004), in Eq. (38), and some simplifications, the impact force for the "i"th impactor is obtained as:

$$F_c^i(t)=\frac{K_c^{i*}V_0^i}{(\phi_2^i-\phi_1^i)}[\frac{1-\phi_2^i}{\omega_2^i}\sin(\omega_2^i t)-\frac{1-\phi_1^i}{\omega_1^i}\sin(\omega_1^i t)] \tag{39}$$

where:

$$\begin{aligned}
\omega_1^{i2}&=\frac{1}{2}(\frac{(N^i+1)K_c^{i*}+K_g^i}{N^iM_I^i}-\sqrt{((\frac{(N^i+1)K_c^{i*}+K_g^i}{N^iM_I^i})^2-4\frac{K_c^{i*}K_g^i}{N^iM_I^i}}))\\
\omega_2^{i2}&=\frac{1}{2}(\frac{(N^i+1)K_c^{i*}+K_g^i}{N^iM_I^i}+\sqrt{((\frac{(N^i+1)K_c^{i*}+K_g^i}{N^iM_I^i})^2-4\frac{K_c^{i*}K_g^i}{N^iM_I^i}}))\\
(\frac{B^i}{A^i})_{\omega_1^i}&=\frac{K_c^{i*}}{K_c^{i*}-M_I^i\omega_1^{i2}}=\phi_1^i,(\frac{B^i}{A^i})_{\omega_2^i}=\frac{K_c^{i*}}{K_c^{i*}-M_I^i\omega_2^{i2}}=\phi_2^i
\end{aligned} \tag{40}$$

where $N^i=\frac{M_{eff}^s}{M_I^i}$. In Eq. (39), K_c^{i*} (i=1,2,...,N) are unknowns and must be obtained. Using Taylor binominal expansion and some mathematical operations, maximum contact time and the corresponding maximum contact force for the "i"th impactor can be written as follows:

$$t^i{}_{\max}=\sqrt{\frac{2N^iM_I^i}{(N^i+1)K_c^{i*}}} \tag{41}$$

$$F_{c\max}^i=\frac{2}{3}V_0^i\sqrt{\frac{2N^iM_I^iK_c^{i*}}{(N^i+1)}} \tag{42}$$

Using Eq. (42) and Choi's linearized form (2004), linearized contact stiffness can be obtained as follow:

$$\mathrm{K_c^{i*}}=(\frac{2\sqrt{2}}{3})^{\frac{2(n-1)}{n+1}}(\frac{N^i}{N^i+1})^{\frac{n-1}{n+1}}(V_0^i)^{\frac{2(n-1)}{n+1}}(K_c^i)^{\frac{2}{n+1}}(M_I^i)^{\frac{n-1}{n+1}} \tag{43}$$

By substituting Eq. (43) in Eq. (39), impact forces can be easily calculated.

3.1 Modified Linearized Contact Stiffness

To obtain the modified contact stiffness (k_{cl}^i), Eq. (44), (Yang and Sun, 1981) must be used. Therefore, in a repeat loop, the contact stiffness for any impactors can be modified. In other words, the first guess for maximum impact force, it can be used from Eq. (42):

$$k_{cl}^i=F_m^{(i)1/3}k_c^{(i)2/3} \tag{43}$$

The process of obtaining the modified linearized contact stiffness is shown in Figure 3.3.

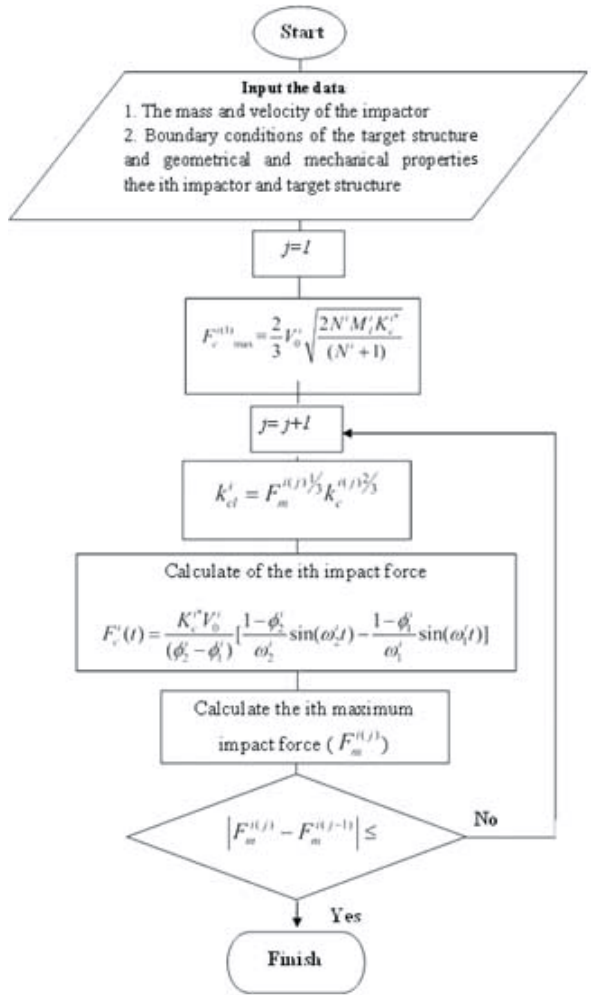

Figure 3.3: Process of modification in the contact stiffness.

4 VALIDATION OF RESULTS AND DISCUSSION

In this section, the numerical results obtained from the presented formulations and impact force models are validated using FE model by ABAQUS code (2008). For modeling the impactor, it is assumed that the it is rigid which means that Young`s module is infinite. This assumption has been used by many researches: Kistler and Waas (1999) and Tarfaoui et al. (2008). In order to model the impact problem by FE methods, it is clear that contact constraints should be used between the target structure and impactor. For contact modeling, there are many contact laws that can be applied in ABAQUS. Failure is predicted with Tsai-Hill criteria and checked it in our program automatically.

SC8R elements are used for the face sheets, while solid elements are used for the core. The impact analysis in ABQAUS is performed in ABAQUS/Standard software, which uses a central difference rule to integrate the equations of motion explicitly. In this study, the face sheets and the foam core were meshed using SC8R and C3D8R elements, respectively.

Here, the clearance between two surfaces (surface of the top face-sheet and surface of the impactor) is considered to be zero and Hertz's contact law is used for over closer between the structure and impactor. First, the cylindrical sandwich panel with composite face-sheets and a foam core with simply supported boundary conditions that is subjected to a single impact at location $(x,\theta)=(L/2,0)$ is studied. Mechanical properties of the sandwich panel and the impactor are given in Table 1.

Sandwich panel with foam core			Impactor	
Properties	Face sheets	Core	Properties	
E_{11}(GPa)	131	0.00689	E(GPa)	200
E_{22}(GPa)	10.34	0.00689	v	0.3
E_{33}(GPa)	10.34	0.00689	Radius (mm)	12.7
G_{12}(GPa)	6.895	0.00345	Velocity (m/s)	3
G_{13}(GPa)	6.895	0.00345	Mass (g)	10
G_{23}(GPa)	6.205	0.00345	$\rho(kg/m^3)$	7960
ν_{12}	0.22	0. 00001	-	-
ν_{13}	0.49	0. 00001	-	-
ν_{23}	0.49	0. 00001	-	-
$\rho(kg/m^3)$	1627	94.195	-	-
$h_t=h_b=3mm, h_c/h=0.88, R_c=10h, L=2R_c,$ layup lamination $[0/90/0/\text{core}/0/90/0]$ (Geometrical properties of the panel)				

Table 1: Material and geometrical properties of the circular cylindrical sandwich panel and impactor.

In Figure 4.1 and Figure 4.2, the converged impact force and deflection histories (m=n=25) are presented, respectively. As seen in Figure 4.1, the history of the impact force obtained from complete and FE models is close and there is little discrepancy between the results from the two presented models. Therefore, it can be concluded that the presented formulations and FE model can be applied to the analysis of the impact on cylindrical sandwich structures. Figure4.2 demonstrates that the deflection histories of the top and bottom face-sheets obtained from complete model are in good agreement with the FE model by ABAQUS code. Also, Figure 4.2 indicates that the deflection of the top face-sheet is higher than that of the bottom face-sheet because of the flexibility of the core. Such difference causes the indentation of the core. These studies show

that the FE model by ABAQUS can adequately predict the impact force and the deflection histories and it is obvious that using FE code is really simpler than other theoretical impact force models, while its accuracy is also quite good.

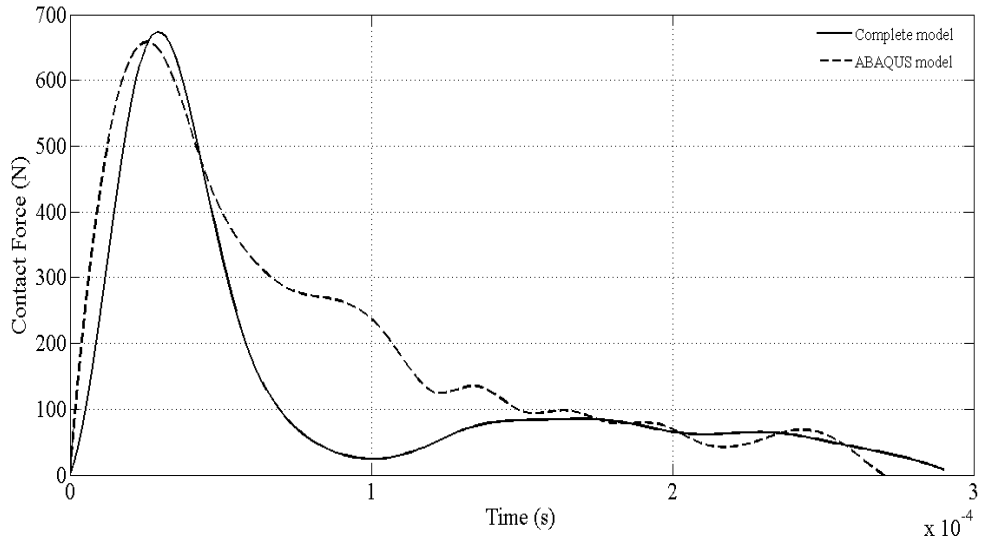

Figure 4.1: Comparing contact force histories obtained from FE and complete models for a circular cylindrical sandwich panel subjected to single small mass impact at location $(x,\theta)=(L/2,0)$ at the first impact location.

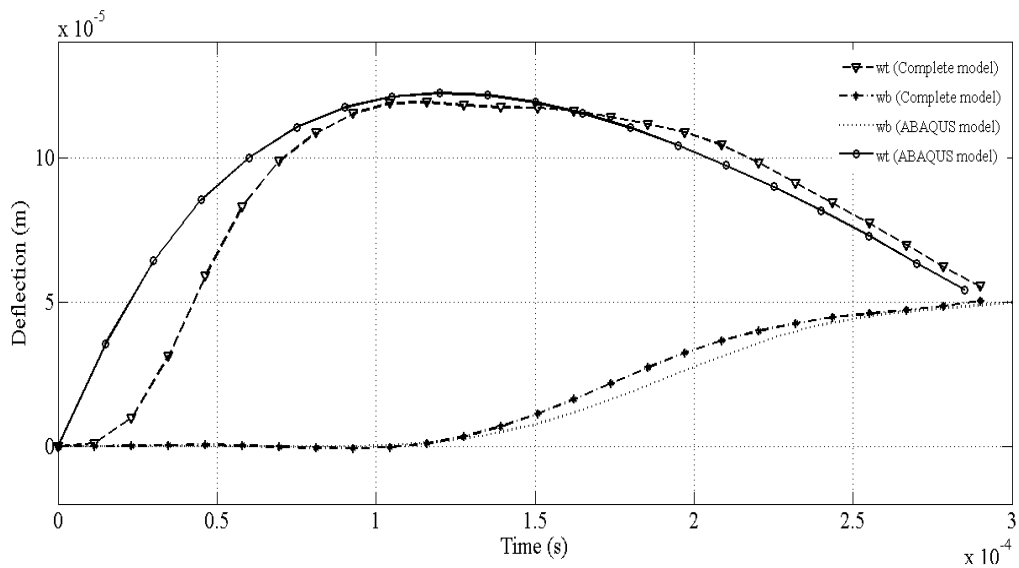

Figure 4.2: Comparing deflection histories of the top and bottom face-sheets obtained from FE and complete models.

Deflection variation of the top face-sheet along x-axis for cylindrical sandwich panel is presented in Figure 4.3. This figure shows that the deflection at the boundary conditions (x=0, 0.6 m) is zero and also it can be seen that the maximum deflection of the top face-sheet occurs at the impact location $(x,\theta)=(L/2,0)$.There are a few studies about the single impact and multiple impact analyses of cylindrical sandwich panels with analytical formulations or FE modeling using finite element software.

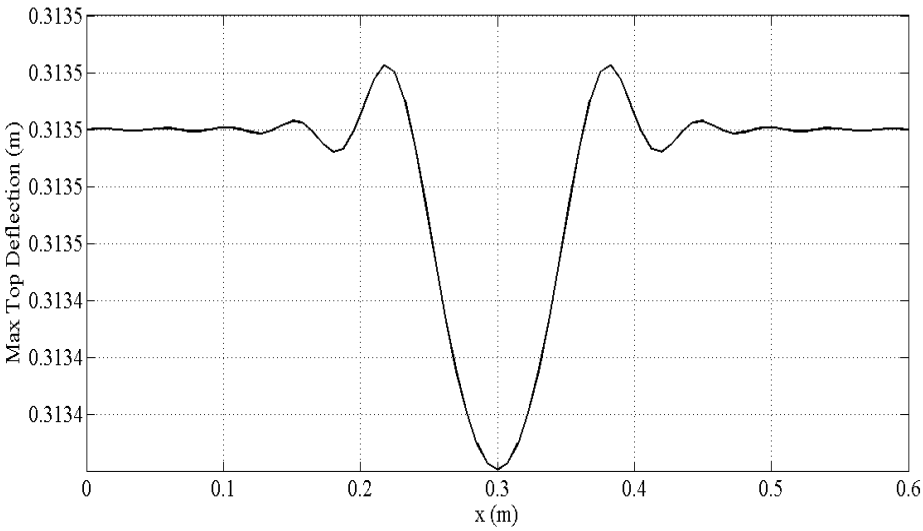

Figure 4.3: Top face-sheet deflection obtained from complete model for a circular cylindrical sandwich panel subjected to single impact.

In this research, the cylindrical sandwich panel subjected to single impact and multiple impacts was modeled by ABAQUS code. As seen earlier, properly good results were derived. As an example, in Figure 4.4 the cylindrical sandwich panel with applied SS boundary condition is shown. FE modeling of the sandwich panel and the impactor is shown in Figure 4.5a and also, in Figure 4.5b, the 3D contour of the deflection of the impactor and the sandwich panel are presented.

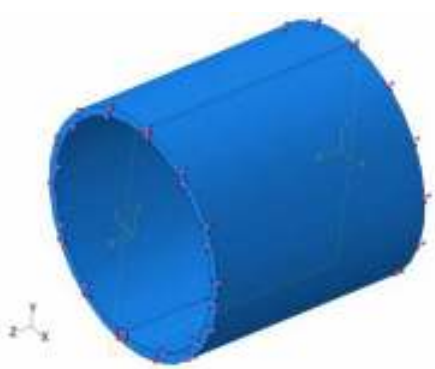

Figure 4.4: Cylindrical sandwich panel with SS boundary conditions along whole periphery.

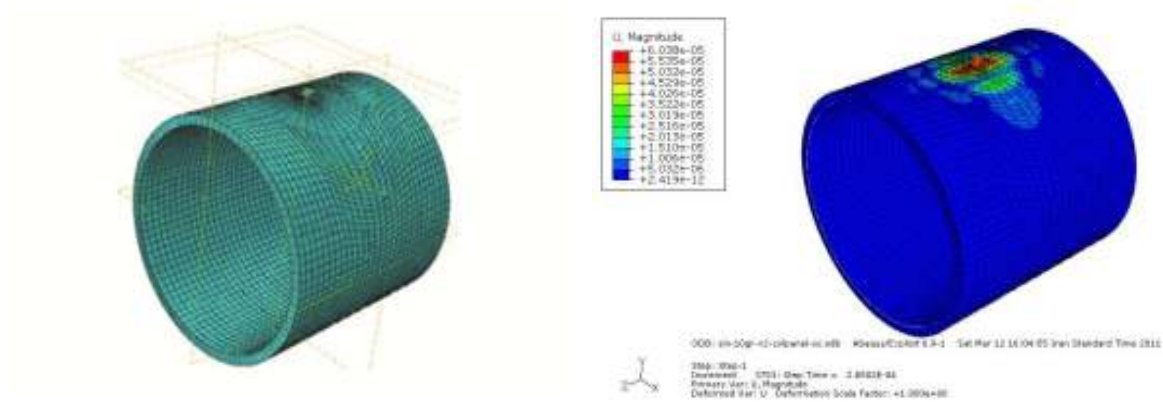

(a) (b)

Figure 4.5: FE modeling and 3D view deflection of a composite sandwich panel and the impactor.

In Figures 4.6 and 4.7, the dynamic response of a cylindrical sandwich panel subjected to two impactors is investigated. It is assumed that the impactors are impacted on the top face-sheet at locations $(x_1, \theta_1) = (L/4, 0)$ and $(x_2, \theta_2) = (3L/4, 0)$. The converged impact force and deflection histories (m=n=25) at location (x_1=L/4 mm, θ_1 =0) are investigated. As seen in these figures, the converged results obtained from complete solution model are in good agreement with the results from FE model by ABAQUS code. Moreover, it can be seen in Figure 4.7 that the deflection of the top face-sheet is more than that of the bottom face-sheet and this behavior occurs due to the core flexibility.

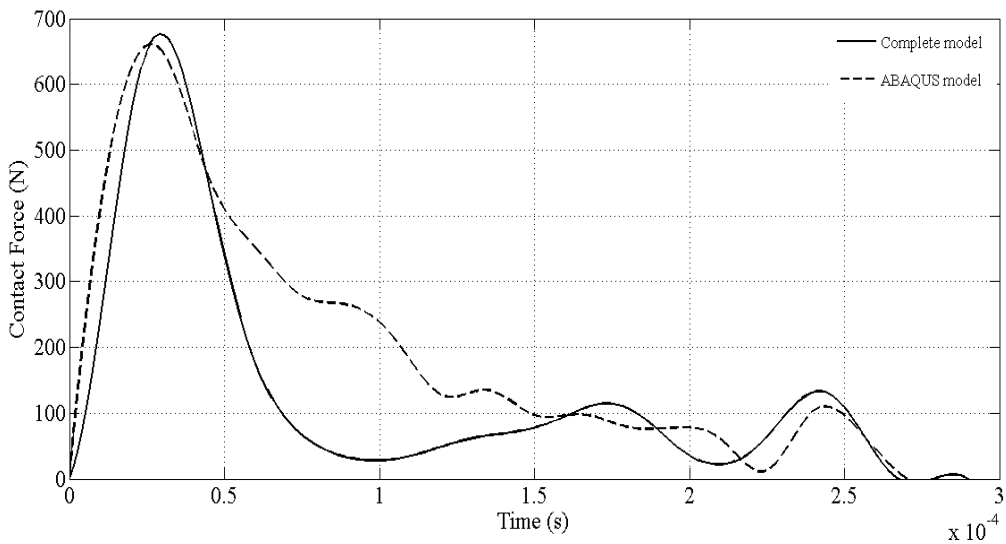

Figure 4.6: Comparing contact force histories obtained from FE and complete models for a circular cylindrical sandwich panel subjected to multiple small mass impacts.

As seen in Figure 4.6, at maximum contact time (t_{max} =2.7e-4s), maximum impact force at each impact location from FE and complete solution models reaches zero; but, the top and bottom face-sheet deflections obtained from these models at t_{max} are not zero. In small mass impacts, maximum contact time for impact force history and deflection history are not equal and the impact force is lower than the deflection history. Different views, i.e. the 3D view and side view, of the deflection based on m=n=25 are presented in Figure 4.8. As can be seen, the impact force and deflections at two impact locations are the same, because the mechanical and geometrical properties of the two impactors are the same and also the distance of the locations of the two impact forces from the midpoint of the sandwich structure is equal.

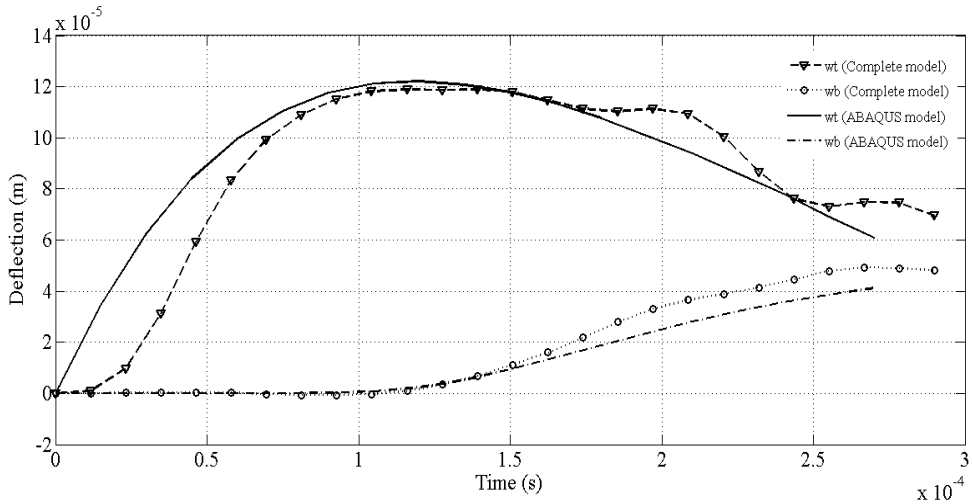

Figure 4.7: Comparing deflection histories of the top and bottom face-sheets obtained from FE and complete models for a circular cylindrical sandwich panel subjected to multiple small mass impacts.

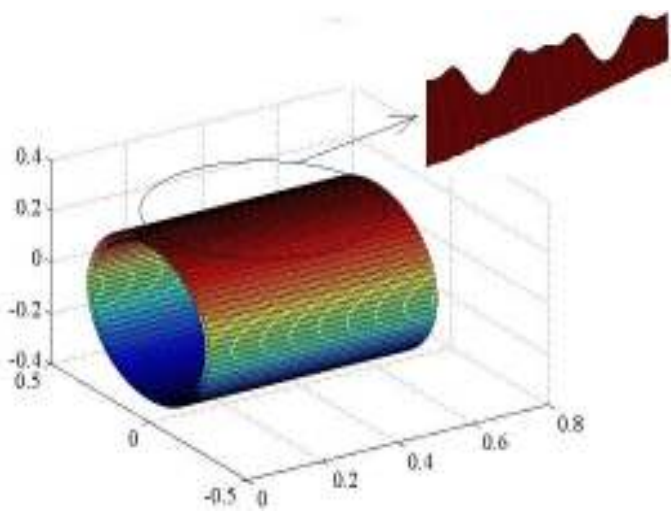

a. 3D view.

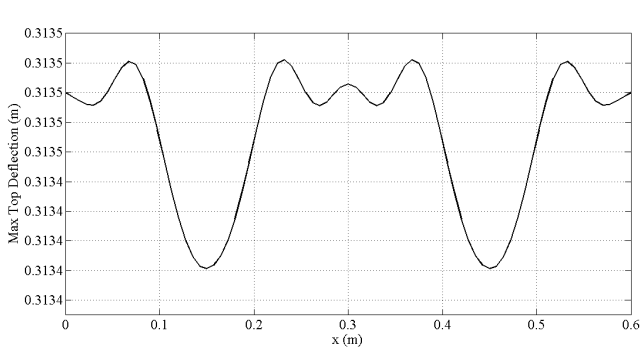

b. Variation of the maximum top deflection.

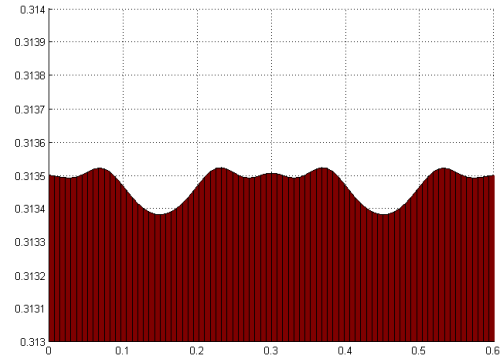

c. Side view of the vertical deflection.

Figure 4.8: Different views of maximum deflection for a circular cylindrical composite sandwich panel with simply supported boundary conditions subjected to two impactors.

In Figures4.9 and 4.10, the converged impact force from both complete solution and TDOF models and also the histories of deflection of the top and bottom face-sheets are presented using three models including complete, TDOF (non-coupled), and TDOF models (coupled with the governing equations of motion) at location (x_1=L/4, θ_1=0), respectively. In this example, the dynamic response of a circular cylindrical composite sandwich panel with simply supported boundary conditions subjected to two impactors is investigated. It is assumed that all the impactors are impacted on the top face-sheet of the panel at locations (x_1=L/4 mm, θ_1=0) and (x_2=3L/4 mm, θ_2 =0). Mechanical properties of the sandwich panel are given in Table and also the geometrical properties of the panel are the same as those of the previous examples. Mass of the impactors is 3kg, while the impact velocity of all the impactors is 3 m/s and their radius is 12.7 mm.

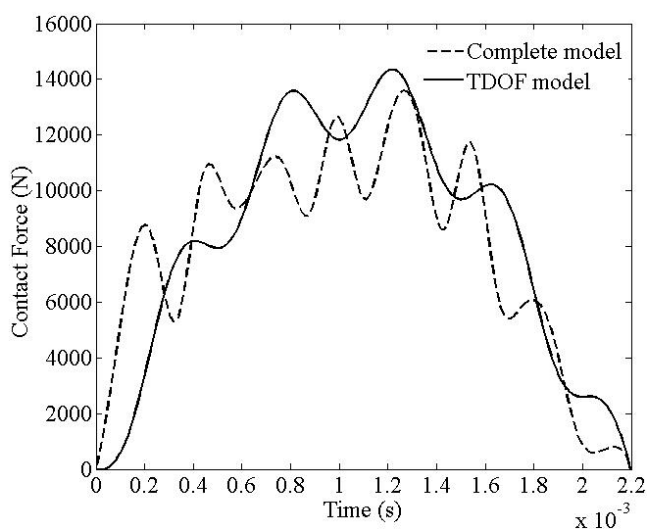

Figure 4.9: Converged impact force obtained from complete and TDOF models for a circular cylindrical composite sandwich panel subjected to two impactors.

Figure 4.11 shows a comparison of maximum transverse deflections of two models (complete solution and TDOF, coupled) at the top and bottom face-sheets through the impact points on the top face-sheet of the panel. As demonstrated in this figure, the results from the two mentioned impact force models are very accommodation and their difference is negligible. Deflection of the top face-sheet is higher than that of the bottom face-sheet due to the flexibility of the foam core. Different views (3D view and side view) of the deflection based on m=n=9 are presented in Figure 4.12.

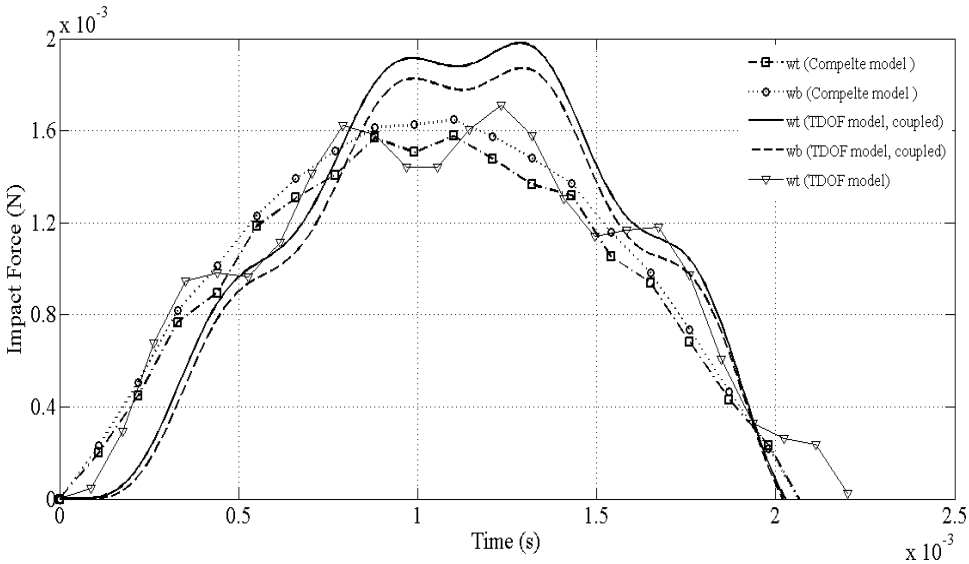

Figure 4.10: The top and bottom face-sheet deflections obtained from complete, TDOF (coupled), and TDOF models for circular cylindrical composite sandwich panel subjected to two impactors.

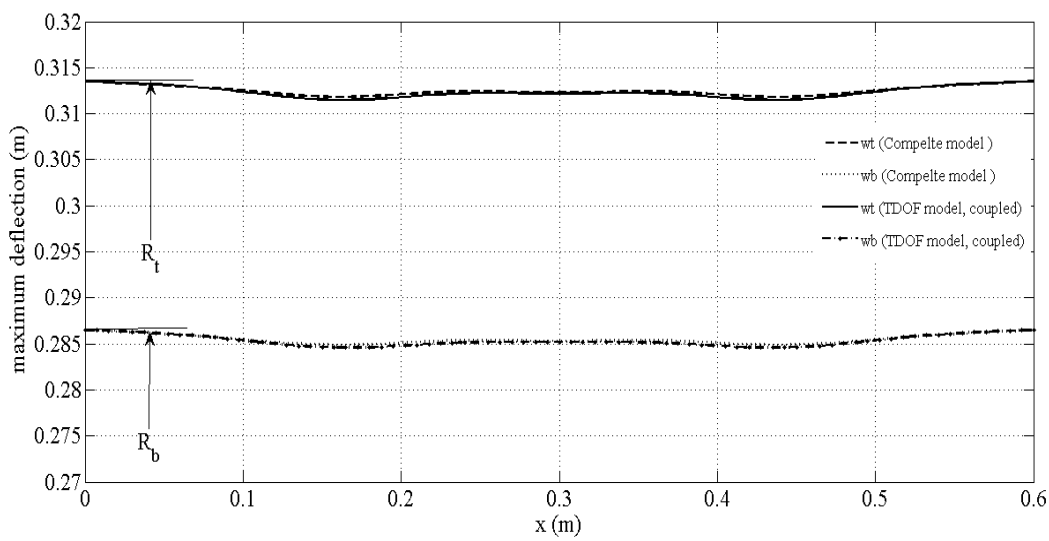

Figure 4.11: Variation of the top and bottom face-sheet deflections obtained from complete and TDOF (coupled) models along x-axis for a circular cylindrical sandwich panel subjected to two impactors.

Some composite structures in practical applications might be impacted by impactors with different masses. Thus, in this section, the dynamic response of a cylindrical circular shell subjected to two impactors with masses m_1 and m_2 is studied and the shell properties are given in Table 2, except that $h_c(mm)$ =24 and Ply Thickness=0.75 are considered. Also, the geometrical properties of the sandwich panel are R_c =10h and $L = 2R_c$ where h is total thickness of the sandwich panel. Index 1 is an impactor with mass m_1 that impacts on the top face-sheet at location (x_1=L/2, θ_1 =0) and index 2 is an impactor with mass m_2 that impacts on the top face-sheet at location (x_2=3L/4, θ_2 =0).It is also assumed that the masses of the impactors are (m_1,m_2)=(m, m), (m_1,m_2)=(2m,3m), and (m1,m2)=(3m,4m) where m=3 kg.

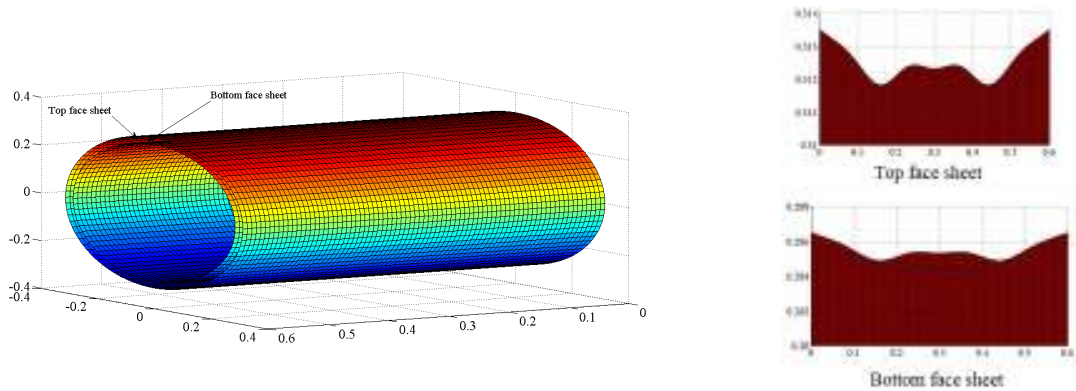

Figure 4.12: Different views of the circular cylindrical composite sandwich panel subjected to two impactors.

Sandwich panel with foam core			Impactor	
Properties	Face sheets (LTM45EL-CF0111Carbon)	Core (110WF)	Properties	
E_{11}(GPa)	54	0.18	E(GPa)	207
E_{22}(GPa)	54	0.18	ν	0.3
E_{33}(GPa)	4.84	0.18	Radius (mm)	12.7
G_{12}(GPa)	3.16	0.07	Velocity (m/s)	3
G_{13}(GPa)	1.87	0.07	Mass (kg)	1.8
G_{23}(GPa)	1.87	0.07	-	-
ν_{12}	0.06	0. 286	-	-
ν_{13}	0.313	0. 286	-	-
ν_{23}	0.313	0. 286	-	-
$\rho(kg/m^3)$	1511	110	-	-
$h_c(mm)$	-	12.7	-	
Ply Thickness (mm)	0.264	-	-	

Table 2: Material properties of the sandwich panel and impactor.

Moreover, the radius of impactors is 12.7 mm and their velocity is 30 m/s. Figure 4.13 and Figure 4.14 show the comparison of the impact force histories at the first impact locations and maximum deflections corresponding to maximum contact time of each of the first impactor along x-axis, respectively. Results are only obtained by the complete solution model. Figure 4.13 indicates the increased contact force for both boundary conditions with the increase of the impactor mass. Also, these figures demonstrate that maximum impact force and contact time for the same impactor mass for clamped support boundary conditions (CC) is higher and lower than (SS) boundary conditions, respectively. Therefore, by increasing the mass of the impactor from m to 3m, at the first impact location, maximum impact force for (SS) and (CC) boundary conditions increases by 46.42% and 54.83%, respectively.

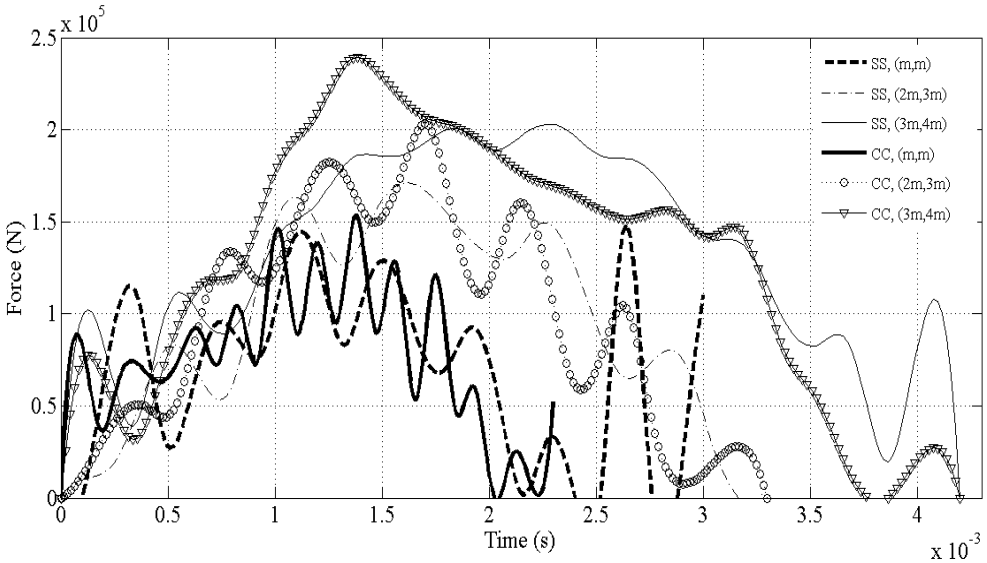

Figure 4.13: Variation of the impact force histories at the first impact location with masses of impactors for a circular cylindrical sandwich panel with SS and CC boundary conditions.

As seen in Figure 4.14, maximum deflection increases for both boundary conditions with the increase of the impactor masses at the two impact locations. As expected, the deflections under the impact locations are maximum. It can be seen in this figure that, for the equal masses of the impactors, maximum deflections at the impact locations are not equal, because the flexibility of the sandwich panel decreases from x=L/2 to x=3L/4. Also, for the same impactor masses, the maximum deflection of the sandwich panel with (SS) boundary conditions is higher than that of (CC) boundary conditions because of increasing the stiffness of the sandwich panel with (CC) boundary conditions.

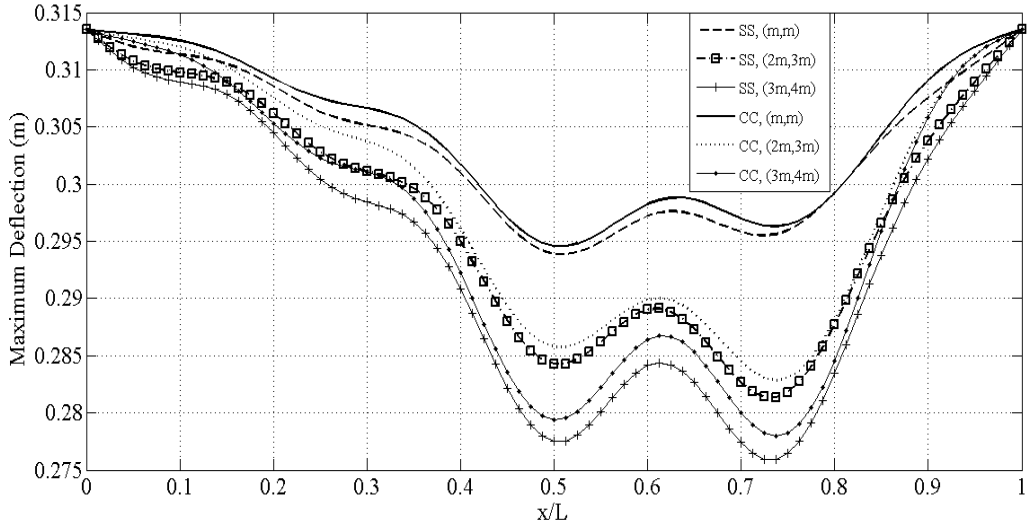

Figure 4.14: Variation of the maximum top face-sheet deflections with masses of impactors at maximum contact time corresponding to the first impactor for a circular cylindrical sandwich panel with SS and CC boundary conditions (variation is along x-axis).

5 CONCLUSIONS

Nowadays, in order to optimum design of structures, engineers usually try to minimize the weight and the cost functions and maximize the structural strength function (fitness function) with optimum selecting of the design parameters. Using standard optimization programs like the commercial Genetic algorithm softwares, one can optimize the design parameters and extermize the fitness functions. The present approach can be linked with the standard optimization programs and it can be used in the iteration process of the structural optimization. The proposed approach facilitates investigation of the effect of physical and geometrical parameters on the transient response of sandwich composite structures subjected to low velocity impact. In this article, at the first time impact analysis of the cylindrical composite sandwich structures was studied based on an improved higher order sandwich panel theory. In order to predict the impact force and other parameters, the new modified analytical spring-mass system with two degrees of freedom (TDOF model) and nonlinear form of Hertz's contact force model (complete solution model) were used. The The validity of a new proposed computational procedure based on improved higher order sandwich panel theory (IHSAPT) and two new analytical models representing contact behavior between the impactors and the panel springs-masses (SM) and nonlinear complete model has been demonstrated by the close agreement between the present computational results and the finite element Abaqus results. Therefore, the problem of impact on the sandwich structures has been simplified to solve a standard structural response equation of motion for a known single ant multi mass impact loading. The effects of mechanical and geometrical properties of the mentioned composite structures and the type of boundary conditions (SSSS and CCCC) on the impact analysis, are investigated.

References

Abrate, S., (2001). Modeling of impact on composite structures. Journal of composite structure 51:129-138.

Chandeashekhara, K., Schroeder, T., (1995). Nonlinear impact analysis of laminated cylindrical and doubly curved shells. Journal of Composite Master 29:2160-2179.

Chai, G. B., Manikandan, P., (2014).Low velocity impact response of fiber-metal laminates. Journal of Composite Structures 107:363-381.

Chai, G. B., Zhu, A., (2011). A review of low velocity impact on sandwich structure. Journal of Material and Application 225:207-239.

Krishnamurthy, K. S., Mahajan, P., Mittal, P. K., (2003). Impact response and damage in laminated composite cylindrical shells. Composite structures 59:15-36.

Choi, I. H., (2006). Contact force history analysis of composite sandwich plates subjected to low velocity impact. Journal of composite structure 75:582-586.

Choi, I. H., Lim, C. H., (2004).Low-velocity impact analysis of composite laminates using linearized contact law. Journal of Composite Structures 66:125-132.

Dassult System's Simulia Crop, (2008). The ABAQUS 6.8-1 User's Manual, USA.

Davar, A., Khalili, S. M. R., Malekzadeh, K., (2013). Assessment of difference higher order theories for low velocity impact analysis of fiber–metal laminated cylindrical shells. Journal of Material, Design and Application DOI: 10.1177/1464420713477348.

Frostig, Y., Thomsen, O. T., (2004). Higher-order free vibration of sandwich panels with flexible core. Journal of Solids and Structure 41:1697-1724.

Hossini, M., Khalili, S. M. R., Malekzadeh, K., (2011). Indentation analysis of in-plane pre-stressed composite sandwich plates: An improved contact low. Journal of Key Engineering Material 471-472:1159-1164.

Hoo Fatt, M. S., Park, K. S., (2001). Dynamic model for low velocity impact damage of composite sandwich panels Part A. Journal of composite structure 52:335-351.

Kang, S. G., Gama, B. A., Yarlagadda, S., Gillespie, J. W., Schutz, T., Fell, S., (2010). Modeling the low velocity impact on thick-section composite cylinder. 11th International Ls-Dyna users conference, Detroit.

Khalili, S. M. R., Azarafza, R., Davar, A., (2009). Transient dynamic response of initially stressed composite circular cylindrical shells under radial impulse load. Journal of composite structure 89:275-284.

Khalili, S. M. R., Malekzadeh, K.,Rahmani,O., (2013). Higher-order modeling of circular cylindrical composite sandwich shell with a transversely compliant core subjected to low –velocity impact. Journal of Mechanics of Advanced Material and Structural DOI:10.1080/15376494.2012.707297.

Kisteler, L. S., Wass, A. M., (1999). On the response of curved laminated beams subjected to transverse impact loads. International Journal of Solids Structures 36:1311-1327.

Krishnamurthy, K. S., (2001).A parametric study of the impact response and damage of laminated cylindrical composite shells. Journal of Science and Technology 61:1655-1669.

Firouzabadi, F., Ayob, A. B.,Moradpour, M., Heidarpour, R., Derriam, N., (2012).Dynamic response of laminated composite cylindrical shell subjected to pure impact. Applied Mechanics and Materials 229-231:2577-2581.

Malekzadeh, K., Khalili, M. R, .Mittal, R. K., (2006). Analytical prediction of low velocity impact response of composite sandwich panels using new TDOF spring-mass-damper model. Journal of composite materials 40:1671-1686.

Matemilola, S. A., Stronge, W. J., (1997). Impact response of composite cylinders. Journal of solids structure 34:2669-2684.

Olsson, R., (2001). Analytical prediction of large mass impact damage in composite laminates. Journal of composite Part A32:1207-1215.

Swanson, S. R., (1992). Limits of quasi-static solutions in impact of composite structures. Journal of Composite Engineering 2:261-267.

Tarfaoui, M., Gning, P. B., Hamitouche, L., (2008). Dynamic response and damage modeling of glass/epoxy tubular structures: numerical investigation. Journal of Composite Part: A 39:1-12.

Timoshenko, S., Goodier, J. N. (1951). Theory of Elasticity. McGraw-Hill, New York.

Willis, J. R., (1966). Hertzian contact of anisotropic bodies. Journal of Mechanics physics solids 14:163-164.

Yang, S. H., Sun, C. T., (1981). Indentation law for composite laminates. Am. Soc. Test. Mater ASTM STP787:425-449.

Damghani Nouri, M.,Hatami, H., (2015). The experimental and numerical investigation of lattice-walled cylindrical shell under low axial impact velocities, Latin American Journal of Solids and Structures 12: Article in Press.